

Paul Chabot

# Study of snow pressure and creep on new support structures located on the Sukkertoppen slope, in Svalbard, Norway

Master's thesis in Nordic Master in Cold Climate Engineering  
June 2022



## DEPARTMENT OF CIVIL AND ENVIRONMENTAL ENGINEERING

---

# **Study of snow pressure and creep on new support structures located on the Sukkertoppen slope, in Svalbard, Norway**

---

TBA4900 - GEOTECHNICAL ENGINEERING, MASTER'S  
THESIS

*Author:*

Paul Chabot

*Co-supervisors:*

Assoc. Prof. Aleksey Shestov - UNIS

Prof. Holger Koss - DTU

Prof. Gudmund Reidar Eiksund - NTNU

June, 2022

---

# Abstract

Avalanches are a growing concern in Longyearbyen, which has led to the expansion of the fields of forecasting and remediation. Snow support structures have to withstand the loads created by the inclined snowpack. The High Arctic town is subject to unique meteorological conditions, this research project aims to assess the relevance of current and previous snow load guidelines for Svalbard and the correlation between snow properties, creep, and pressures. In addition, special attention was to be paid to newly built snow support structures, by assessing the snow loads building up on them. However, the inability to obtain site-specific data greatly diminished the possible analysis of these structures. Therefore, data were collected by a snow load device, located on a slope above the airport, with the same exposure as the structures, and coupled with in-situ density and creep measurements over spring 2022. Among the parameters influencing snow loads, the results showed that fluctuations in temperature gradient and creep rates appear to influence the load variations over a season. However, the total magnitude of the maximum load is largely controlled by the snow height and density. Readings of different creep speeds over the height of the snow-pack were correlated with the higher measured load data on the upper part of the device than on the lower. The estimation of loads by the models gave variable results. Guidelines from Switzerland showed an underestimation of the loads for low snow heights, but an overestimation the higher the snow height, due to squaring the snow height. On the other hand, standards from Norway showed results closer to the data collected by the device. Their approach was more fitting given their work on maritime snow pressure data. The results obtained from this study showed the compliance with the Swiss and Norwegian standards for the cases for the height of the structures implemented in Longyearbyen. However, the fast-changing climate on the island may substantially affect the properties of the snowpack and lead to new snow and pressure distributions on slopes.


---

# Preface

The work presented thesis is part of the joint MSc program Cold Climate Engineering and was carried out at the University Centre of Svalbard (UNIS) in spring 2022. The thesis has been done in collaboration with the Norwegian University of Science and Technology (NTNU) and the Technical University of Denmark (DTU). The supervisor at UNIS, was Assoc. Prof. Aleksey Shestov, with co-supervision from Prof. Gudmund Reidar Eiksund (NTNU) and Prof. Holger Koss (DTU). The work counts for 30 ECTS for 20 weeks. An extra week has been allocated to compensate for completing the *Arctic Survival and Safety* course, which is necessary for fieldwork in Svalbard. The entire fieldwork campaign was carried out in cooperation with Simon Prochaska, a guest master's student from the University of Munich. The idea for the thesis arose from a discussion with Aleksey and Simon about a common interest in Arctic snow creep and the instrumentation of the newly installed snow support structures on Sukkertoppen.

Longyearbyen - June 2022

Paul Chabot



---

# Acknowledgement

I would like to thank all my supervisors, Aleksey, Holger, and Gundmund for their comments and help in the administrative organization of the thesis.

Especially Aleksey Shestov for all the help, valuable input, and the possibility to work with a lot of autonomy.

Simon Prochaska, for sharing the joys of fieldwork in Svalbard, all the exchanges that allowed me to progress in the thesis, and time spent mountaineering in our free time.

Last but not least, all the people with whom I shared the most exciting year of my life!

Thank you all for being such good friends, with the same appetite for mountains and *sometimes* parties, Carlo, Ole Petter, Zimon, Arthur, Solveig, Amish, Saskia, Yannika, Malin, Kristin, Elias, and all of the others!

*In case of doubt, straight it*

---

# Table of Contents

<b>Summary</b>	<b>i</b>
<b>Preface</b>	<b>ii</b>
<b>Table of Contents</b>	<b>vii</b>
<b>List of Tables</b>	<b>viii</b>
<b>List of Figures</b>	<b>x</b>
<b>Abbreviations</b>	<b>xi</b>
<b>1 Introduction</b>	<b>2</b>
1.1 Area . . . . .	4
1.2 Metamorphism and creeping . . . . .	5
<b>2 Theoretical Framework</b>	<b>6</b>
2.1 Objectives . . . . .	6
2.2 Modeling History . . . . .	7
2.2.1 Bucher - 1948 . . . . .	7
2.2.2 Reviewing work - Mellor . . . . .	12
2.2.3 Reviewing work - Salm . . . . .	14
2.2.4 Parametrization of Temperature - Teufelsbauer . . . . .	20
2.3 Poisson's ratio . . . . .	21
2.4 Laboratory experiments - Two approaches . . . . .	23
2.4.1 De Quervain . . . . .	23

---

2.4.2	Abe . . . . .	23
2.5	Swiss guidelines . . . . .	24
2.6	Norwegian standards . . . . .	28
2.7	Case-Studies - In-situ data collection . . . . .	28
2.7.1	McClung & Larsen - Norway . . . . .	28
2.7.2	Wyoming . . . . .	31
2.8	Summarizing table . . . . .	33
<b>3</b>	<b>Methods</b>	<b>35</b>
3.1	Hazard linked to fieldwork . . . . .	36
3.2	Snow Load Device System . . . . .	37
3.3	Snow creep measurement . . . . .	38
3.3.1	Caselli's comparison of set-ups . . . . .	38
3.3.2	Preparation and set-up . . . . .	39
3.3.3	Monitoring . . . . .	40
3.3.4	Errors sources . . . . .	41
3.4	Snow pits . . . . .	41
3.4.1	Description of the different tests . . . . .	41
3.4.2	Errors sources . . . . .	43
3.5	Implementation in-situ testing . . . . .	43
<b>4</b>	<b>Results: in-situ data</b>	<b>44</b>
4.1	Snow pits . . . . .	45
4.1.1	Density . . . . .	45
4.1.2	Temperature . . . . .	46
4.2	Snow load device system . . . . .	48
4.2.1	Snow thickness . . . . .	48
4.2.2	Snow load . . . . .	49
4.2.3	Snow temperature . . . . .	51
4.3	Snow creep . . . . .	54
4.4	Correlation Study . . . . .	57
<b>5</b>	<b>Models interpretation</b>	<b>60</b>
5.1	Density from Snow-pits . . . . .	61
5.2	Site Characteristics . . . . .	63
5.2.1	Common parameters . . . . .	63
5.2.2	Site: Snow load device . . . . .	64



---

5.2.3	Site: Snow supporting structures . . . . .	66
5.3	Models evaluation . . . . .	67
5.3.1	Shooting range . . . . .	67
5.3.2	Sukkertoppen . . . . .	70
<b>6</b>	<b>Conclusions &amp; Further work</b>	<b>72</b>
	<b>Bibliography</b>	<b>73</b>
	<b>Appendix</b>	<b>78</b>
6.1	Appendix A . . . . .	78
6.2	Appendix B . . . . .	79
6.3	Appendix C . . . . .	80
6.4	Appendix D . . . . .	82
6.5	Appendix E . . . . .	84

# List of Tables

2.1	Poisson's coefficient formulate in the literature . . . . .	22
2.2	Creep factor definition from Swiss Guidelines (2007) . . . . .	26
2.3	Summary table of slope-parallel pressures models . . . . .	33
2.4	Summary table of back-pressure models . . . . .	33
4.1	Data collection season . . . . .	44
4.2	Temperature period from data collection . . . . .	52
5.1	Density differentiation based on snow-pack depth . . . . .	62
5.2	Invariant parameters for both sites . . . . .	64
5.3	Snow load device site characteristics . . . . .	65
5.4	Sukkertoppen site characteristics . . . . .	67
5.5	Load calculation Sukkertoppen snow support structures . . . . .	70

# List of Figures

1.1	Longyear Valley location . . . . .	4
2.1	Relaxation time measurement Kuhn, Bucher (1948) . . . . .	9
2.2	Snow-pack development by successive snow fall, Bucher (1948) . . . . .	10
2.3	Creep pressure $S_1$ as a function of snow thickness, $d$ , and slope angle, $\psi$ .	12
2.4	Burger's model from Mellor (1975) . . . . .	13
2.5	Definition of velocities inside the snowpack . . . . .	18
2.6	Viscous analogue envelope, Teufelsbauer (2011) . . . . .	22
2.7	Creep measurements during Abe's experience on the left and computed results on the right . . . . .	24
2.8	Table containing glide factor for different ground roughness and slope exposure, Swiss Guidelines (2007) . . . . .	26
2.9	Schema of the monitored structure from Larsen et al. (1985) . . . . .	29
2.10	Pressure distribution over the structure from strain gauge data - maximal pressure, $\sigma_m$ and mean pressure, $\bar{\sigma}$ , are represented . . . . .	30
2.11	12 days snow pressure monitoring over southern edge of support . . . . .	32
2.12	Evaluation of averaged pressures over the cross beam section . . . . .	32
3.1	Location of both monitored sites in Longyearbyen . . . . .	36
3.2	Snow load testing system implemented in the shooting range site, source: <a href="http://158.39.149.181/Snow_wall/index.html">http://158.39.149.181/Snow_wall/index.html</a> . . . . .	37
3.3	Creep measurement set-up . . . . .	40
3.4	In-situ testing: snow-pits . . . . .	42
3.5	Position of snow-pits and creeping stakes near the snow load device . . . . .	43

---

4.1	Snow density with error bars - Spring 2022 . . . . .	46
4.2	Temperature measured in the pits - Spring 2022 . . . . .	47
4.3	Snow depth data extracted from the Sonic distance sensor . . . . .	48
4.4	Uniform load scheme . . . . .	50
4.5	Uniform load for both Springs . . . . .	50
4.6	Evolution of uniform load during Spring 2022 . . . . .	51
4.7	Snow & air temperature measurements during Spring 2020 . . . . .	52
4.8	Temperature gradient calculated for 140cm snowpack - Spring 2020 . . .	53
4.9	Creep calculation and movement . . . . .	55
4.10	Results - In-situ creep measurement . . . . .	56
4.11	Creep velocities parallel to slope for the upper part . . . . .	57
4.12	Airport Weather Station - Average air temperature - Spring 2022 . . . . .	58
5.1	Snow densities curves, define by snow thickness . . . . .	62
5.2	Poisson's ratio, $\nu$ , in function of snow temperature and density in 2020's spring . . . . .	63
5.3	Sukkertoppen snow support structures . . . . .	66
5.4	Research-oriented models compared to both springs data . . . . .	68
5.5	Guidelines models compared to both springs data . . . . .	69
6.1	Location of Svalbard archipelago . . . . .	78
6.2	Load cells - Spring 2020 . . . . .	79
6.3	Load cells - Spring 2021 . . . . .	79
6.4	More realistic load distribution over the studied plate . . . . .	80
6.5	Creep calculation . . . . .	82
6.6	Poles broken - North side . . . . .	83
6.7	Stake n°1 breakage - June 2022 . . . . .	83
6.8	Rain event - Airport Weather Station - March 2022 . . . . .	84
6.9	Wind speed - Airport Weather Station - March 2022 . . . . .	84

---

# Abbreviations

A	=	Lateral distance between two structures [m]
a	=	Coefficient representing compaction of snow [-]
$a_3$	=	Constant defined for velocity calculation in Bucher (1948)
$C_D$	=	Deformation coefficient in neutral zone [-]
D	=	Snow thickness [m]
$D_k$	=	[m]
$D_{er}$	=	Critical thickness [m]
D*	=	Geometrical component [m]
$E_{M/K}$	=	Elastic modulus for Maxwell and Kelvin-Voigt unit [Pa]
$E_d$	=	Design effect of loads [kN/m]
$f_R$	=	End-effect factor [-]
$f_s$	=	Yield stress [Pa]
G	=	Shear modulus [Pa]
g	=	Gravitational acceleration [ $m/s^2$ ]
H	=	Snow height [m]
K	=	Creep factor [-]
k	=	Shear yield strength [Pa]
$K_p$	=	Factor characterising the loose or compact nature of snow [-]
L/H	=	Creep parameter [-]
m	=	Ratio of the longitudinal to the lateral rate of deformation in the uni-axial state of stress, Sal
N	=	Glide parameter [-]
N	=	Glide factor [-]
n	=	Relative glide velocity [-]
$Q_k$	=	Snow load [kN/m]
$R_k$	=	Material resistance [kN/m]
$r_T / r_\rho$	=	Constants [-]
$S'_N$	=	Normal stresses applied on the structure [Pa]
T	=	Snow temperature [°]
$T_r$	=	Relaxation time [s]
u	=	Creep velocity parallel to slope [m/s]
$u_0$	=	Creep velocity parallel to slope at $x = 0$ [m/s]
v	=	Creep velocity normal to slope [m/s]
$v_g$	=	Creep velocity normal to slope at $x = 0$ [m/s]

$v_0$	=	Gliding velocity [m/s]
$y_b - L_{er}$	=	Back-pressure zone [m]
$z$	=	Snow-pack depth studied [m]
$\beta$	=	Creep angle, i.e. angle between u and v vectors direction [°]
$\gamma - \rho$	=	Snow density
$\gamma_Q$	=	Safety factor load [-]
$\gamma_M$	=	Safety factor material [-]
$\Delta l$	=	Lateral length of application of end-effect [m]
$\eta$	=	Snow viscosity [Pa/s]
$\nu$	=	Poisson ratio [-]
$\nu_{max}$	=	Maximal value of $\nu$ [-]
$\rho_p$	=	Density where $\nu(\rho, T)$ changes curvature [ $\text{kg}/\text{m}^3$ ]
$\rho_p^0$	=	Density at the upper boundary, where $T = 0^\circ\text{C}$ [ $\text{kg}/\text{m}^3$ ]
$\tau$	=	Shear stress [Pa]
$\psi$	=	Slope angle [°]

# Chapter 1

## Introduction

Avalanches have always been a major hazard for structures and people in snowy mountainous environments. The Arctic settlement of Longyearbyen has experienced a growing and forced interest in this topic. This has been due to the repeated and worsening avalanche damage in recent years. However, the risk is not new, in 1957 an avalanche swept away a large part of the hospital, killing three people in the process, Hestnes (2018). It is the tragic event of December 2015 that has raised more awareness of the danger among locals and authorities. On 19 December 2015, an avalanche was released at the top of the slope called "Lia", overlooking the town to the east, Indreiten (2018). The avalanche swept away several houses in its path and killed two people. On the same slope, a second avalanche occurred in 2017, but smaller and caused no human casualties.

After these critical events, significant interest was shown in the study and forecasting of avalanches in Svalbard, leading the town to set standards for forecasting in mainland Norway, Eckerstorfer (2013). As a result, research and instrumentation of the slopes around the town have increased significantly. Political will and unblocking of funds have led to reflections on methods of remediation. The implementation and design of defense structures require a good understanding of snow behavior and avalanche triggering.

Snow science can be designated as a relatively young science, with significant development in the 1980s. The engineering design of structures exposed to seasonal or continuous snow pressure is even more recent. A guideline published by the Swiss Federal Institute (SLF), and translated into English in the 2000s, has served as an internationally recognized guideline. Most of the engineering offices have based themselves on the Swiss recommendations for the calculation of loads on snow-bearing structures. Yet, several countries, such as, Hewes et al. (2016) (USA), Harada (2014) (Japan), Larsen (2000) (Norway), have col-

---

lected their own snow pressure data in order to establish adaptations of the standard to their environment. Following this example, the question of the differences in the build-up of pressures from a snowpack located in Svalbard emerges.

Indeed, the meteorological, geological, and, to a certain extent, extreme conditions present on the archipelago, push towards a study of the possible differences with the models thought for alpine snow. Svalbard is also experiencing a higher rate of global warming than anywhere in the world, Overland et al. (2019). The summer of 2020 and the spring of 2022 were the warmest ever recorded in the city. Monitoring the effects of these changes on the snowpack will be of great interest in the years to come.

With this work, I will try to evaluate whether the snow loads on structures generated by the Svalbard snowpack are comparable to the standards and models developed over the years. The initial aim was to establish a plate with pressure sensor cells on the structures in Sukkertoppen. But complications with contacting and obtaining permission from the company that built/designed them delayed the possible implementation. The load measurement plate was also to be manufactured in collaboration with the Logistics department at UNIS. Based on these measurements, it would have been possible to adopt a more design and engineering-oriented approach, where the measured loads/pressures could have been directly compared to model predictions and analyze the performance of the structural design.

Instead, a more research-oriented approach was taken. The choice was made to use the data provided by a snow loading system, located on a slope with the same exposure, above the airport, Alberg (2019). The device was installed in autumn 2019 and the collection of pressure data, and other parameters, are available for UNIS's research. To gather in-situ snowpack parameters, such as density, hardness, and creeping, a fieldwork campaign has to be held every week between February and May 2022. These different parameters will be compared, the aim is to evaluate correlations between weather, snow temperature and density, and loads.

Chapter 2 presents a detailed review of the state of snow science and the models used to predict snow pressures. Chapter 3 outlines the methodology of the in-situ tests carried out. Chapter 4 reports the results, which will be discussed in Chapter 5. While Chapter 5 also includes a presentation of the necessary site characteristics used by the models. Chapter 6 concludes and mentions further work for this thesis. The next two paragraphs will present the study area and key concepts of snowpack development.



## 1.1 Area

Longyearbyen is located on the Spitsbergen island in the Svalbard archipelago. This Norwegian territory is the northernmost in the world, see Appendix 6.1. The town area is considered to be an arctic desert (rainfall  $\leq 200\text{mm/year}$ ), with approximately 150mm of rain a year, Christiansen et al. (2013). Therefore, the main reasons for avalanches are generally not caused by heavy snowfall, but rather by large snow drifts and accumulation on slopes. It is therefore of paramount importance to be aware of the direction of the prevailing winds. In Svalbard, the valleys play an important role in channeling the wind, Lonardi (2018). In the valley of Longyearbyen (i.e. Longyeardalen), the prevailing wind direction is coming from the south. While at the airport station, the prevailing wind is from east to west, channeled through the wide Advent valley (i.e Adventdalen), see figure. 1.1. The east-west wind direction is dominant over most of the island, which is subject to the perturbation caused by the topography. As a result, the accumulation side, i.e. Leeward, is often West oriented slope, such as "Lia".

Longyearbyen town: Structures and valleys relevant to the study

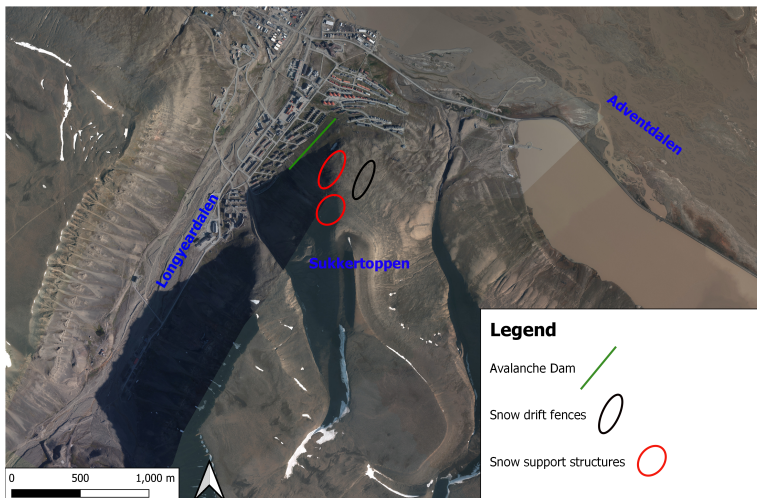


**Figure 1.1:** Longyear Valley location

Avalanche-prone slopes range from  $25^\circ$  to  $55^\circ$ , McClung and Schaerer (2006). 94% of 200 slab avalanches studied by Perla (1977) were triggered at a slope angle above  $30^\circ$  and below  $45^\circ$ . The slope studied, "Lia", is located on the mountain "Sukkertoppen". The avalanche barrier rows and the dam are shown in the figure 1.1. The first shoulder has an altitude of 150m and the top of 300-350m. The slope varies from  $30^\circ$  to  $40^\circ+$  and has a

western exposure. Construction is still underway, with the highest rows being put in place during the fall of 2021 and spring of 2022.

## 1.2 Metamorphism and creeping

Dry snow-pack is classified as an aggregate of snow crystals, Sommerfeld and LaChapelle (1970). Even if Longyearbyen is the northern-most city in the world, the snowpack is seasonal here, and properties of such are taken. Snow crystals are formed in the atmosphere during a process of super-cooling of water droplets creating supersaturation and crystals grow as needles, Colbeck (1987).

When deposited on the ground, the crystals will transform under changes in properties and time, Singh (2011). The factor influencing the whole metamorphism process is the temperature gradient. The ground temperature is near the melting point of snow ( $0^{\circ}\text{C}$ ) due to geothermal heating and summer stored heat. Temperature reduces when closing up to the surface, exposed to winter temperatures. The warmer the saturated air, the more vapor it can hold, resulting in higher vapor pressure near the bottom of the snowpack, claims McClung and Schaerer (2006). This creates a vapor pressure gradient and the vapor is forced upwards (vertical flow of heat and vapor in the snow cover). Vapour diffusion occurs by evaporation and condensation from one crystal to another. The rate of motion, i.e. metamorphism, controls the type of crystals formed and is controlled by the temperature, its gradient, and pore space. The greater the temperature gradient and the larger the pores, the more faceted the crystals will be. On the contrary, a low-temperature gradient will tend to produce more rounded grains. Faceted layers have poor bonding between the grains and other layers, receiving the name "weak layer". They are responsible for most of the dry snow avalanches (i.e. slab) triggering. As a rule, the limit between low and high-temperature gradient has been set to  $10^{\circ}\text{C}/\text{m}$ , McClung and Schaerer (2006).

In the context of structures in slopes, snow loads are controlled by density and slow motion, i.e. creeping, of the snow-pack. Creep phenomena are very important for the build-up of snow loads. It is always present in the snowpack, due to its high porosity and metamorphism processes, McClung and Schaerer (2006). Creeping is held responsible for 90% of density and hardness increase inside the pack, by re-arranging the grains. Therefore, creep-induced loads are generally considered to be critical for the design of snow-supporting structures, McClung and Larsen (1989). The creeping process will be explained in more detail in the next section.

# Theoretical Framework

## 2.1 Objectives

Issues management related to avalanches and snow loads on structures is not a new topic for high altitude and arctic regions. However, the study of snow properties and mechanics is relatively recent. The first approach was aimed at defining snow as a material and its pressure acting on structures. It comes from the Swiss research field. At the end of the 1930s and during the 1940s, the Swiss scientists Bader, Haefeli, and Bucher, each published papers on snow mechanics. These publications have been fundamental to future research and attempt to formulate snow pack behavior and creeping. Unfortunately, the papers are dated and written in German. Despite being cited in the majority of recent publications, I have only been able to find one complete paper from Bucher (1948)'s work. It has been translated to English by an online translator.

This section's goal is to establish a theoretical framework of snow pressure and load modeling. It examines the stages in the history of snow modeling, from the first models to the directions taken for engineering purposes. Priority interest is given to snow loads due to the interruption of snowpack movement by defensive structures on slopes.

The first part focuses on the different models developed over the years, their assumptions, their limitations, and their implications.

A second part is devoted to the work done in laboratories, to establish empirical relationship between pressure, settlement, temperature, and the density of the snow. It is used for model validation and provides data for future models.

Then, the Swiss Guidelines (2007) are presented. As mentioned earlier, they are now the

reference standard for the construction of snow support structures all around the world. The equations and safety factors of this standard were determined from experience on alpine snow. Norwegian standards, Norem (2014), have tackled the specificity of a snowpack in a maritime environment. Using snow pressure data collected in Norway, they formulated a multiplication factor to account for the particularity of Norwegian fjords. And finally, two studies monitoring in-situ snow pressure on structures will be analyzed. In both cases, the snow support structures were monitored with pressure cells and strain gauges. The studies are separated by thirty years and are located in Norway, Larsen et al. (1985) and Wyoming, USA, Hewes et al. (2016).

## 2.2 Modeling History

As indicated, much of the early modeling work, which formed the basis for the current models, is not available online. However, the reviewing work of Mellor (1975), Salm (1977) and Shapiro (1997) have given an idea of their bearing and approach to snow behavior in the early days. Nevertheless, Bucher (1948)'s paper is a good example of the state of snow mechanics in its early stage and will be introduced first below.

### 2.2.1 Bucher - 1948

#### Model definition - Elasto-plastic law

Bucher published 1948, an important work on the behavior and mechanics of snowpack, which can be translated as "Contribution to the theoretical principles of avalanche shoring". His work refers to the contemporary work of Haefeli and Bader which I did not have access to but which will be referenced as they were in his paper. Bucher (1948) described the snow as a viscous and compressible aggregate whose properties are highly dependent on temperature and density. In particular, as it approaches its melting temperature ( $0^{\circ}C$ ), the ice crystals gain freedom of movement and tend towards a viscous behavior, said Bucher. During the first attempts to model the deformations of snow, an elastoplastic law was used, i.e. involving reversible elastic deformation and a yield point beyond which the deformation is plastic and non-reversible. To apply this law, elastic and plastic behaviors are specified separately. They are defined according to Hooke and Newton, respectively:

$$\gamma = \tau \cdot \frac{1}{G} \quad [Elastic : \quad Hooke] \quad [-] \quad (2.1)$$

$$\frac{d\gamma}{dt} = \frac{1}{\eta} \cdot \tau \quad [Plastic : \quad Newton] \quad [-] \quad (2.2)$$

The deformation rate in the transition zone is described by a Bingham law, combining elastic and plastic behavior:

$$\frac{d\gamma}{dt} = f_s \cdot (\tau - f_s) \quad [-] \quad (2.3)$$

With  $\gamma$  [-] is the angular variation, it corresponds to the angle variation of the deformed snow block, and can be seen in the figure. 2.1.  $G$  [Pa], is the shear modulus,  $\tau$  [Pa] represents the shear stress,  $z$  [m] is the snow depth, and  $\eta$  is the "Toughness" of the material, meaning the resistance of a material to fracture and crack propagation.  $f_s$  denotes the yield point or limit of the stress of the material, which represents the limit between elastic and plastic behavior.

The viscous behavior of snow introduces the major concept of creep. In a laboratory context, creep corresponds to the increasing deformation of a material under a constant load. As previously said, it is one of the main drivers of the build-up of snow load on structures, and its contribution to the sum of pressures will be discussed further.

### Relaxation time

Another concept presented is relaxation time. It corresponds to the time required for the stresses to decrease to zero while the deformations are held constant. Holding the strain constant, elastic behavior is observed first, then the stress decreases until it becomes zero. It is introduced as a means of estimating the amount of elastic and plastic deformation that the sample has undergone.

To take into account the influence of temperature and process history/loading of the sample, leading the snow to behave as a viscous fluid, Bucher (1948) reused the equation formulated by Maxwell in 1867:

$$\frac{d\gamma}{dt} = \frac{d\tau}{dt} \cdot \frac{1}{G} + \frac{\tau}{\eta} \quad [Maxwell] \quad [-] \quad (2.4)$$

An assumption of constant displacement is made. This means that  $\gamma$  is constant and  $\frac{d\gamma}{dt} = 0$ . Therefore, Maxwell equation can be equalized to zero. Thus a solution of the equation is of the form,

$$\tau = \tau_0 \cdot e^{-\frac{G}{\eta} \cdot t} \quad [Pa] \quad (2.5)$$

This allows the relaxation time,  $T$ , to be introduced as a ratio of viscosity and shear modulus,  $T = \frac{\eta}{G}$  [s].

Kuhn (1939) performed relaxation time measurements by varying the toughness  $\eta$  in the temperature range from  $-40^{\circ}\text{C}$  to  $0^{\circ}\text{C}$ . His results are shown in the figure, 2.1:

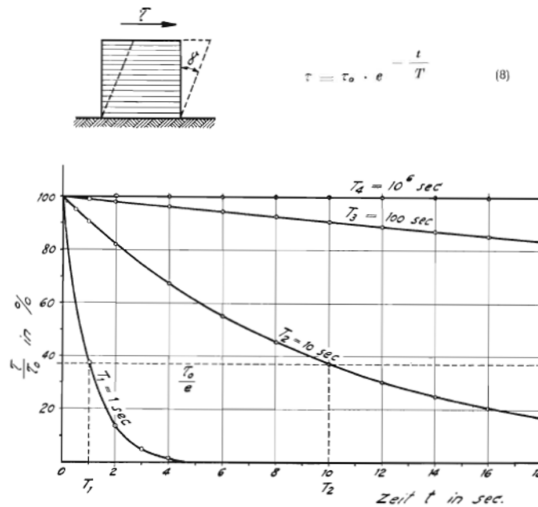


**Figure 2.1:** Relaxation time measurement Kuhn, Bucher (1948)

*Figure description:* x-axis: Time in seconds, y-axis: Relative shear stress, 4 temperature samples:  $T_1$  ( $-40^{\circ}\text{C}$ ),  $T_2$  ( $-20^{\circ}\text{C}$ ),  $T_3$  ( $-10^{\circ}\text{C}$ ), and  $T_4$  ( $-5^{\circ}\text{C}$ )

This shows the strong dependence of relaxation time on snow temperature and toughness. The closer the snow temperature is to zero, the longer the relaxation time. The relaxation time has a magnitude range of  $10^6$ , characterizing large discrepancies in snow's response, over a wide temperature range.

### Study of influencing factor for snow creep

One of the first approaches to the snow creeping process was carried out experimentally by De Quervain, see chapter 2.4.1 and then by Haefeli. From a simple experiment of snow settling as a function of time, it was determined that the final height is controlled by the minimum porosity and three grain reorganization processes: 1. displacement of individual crystals, 2. surface deformation of crystals, and 3. internal deformation of crystals.

### First approach of snow-pack modeling

The first definition of snowpack and basic laws of snow change was considered by Bucher (1948). The concept of layer dissolution is introduced. This is the principle that snow aggregates become coarser, relatively non-plastic, and poor in cohesion when compressed.

The snowpack has been defined as a superposition of layers with variable properties. The first one is characterized in more detail because it is in direct contact with the ground. In the case of frozen ground with low temperature, there is almost no compression within the layer, and the whole aggregate will become coarse-grained.

In the opposite case of warm soil, the lower part of the layer will undergo strong compression due to high plasticity. After the structure of the model is based on successive snowfall. The figure, 2.2 shows an example diagram for 3 different snow events:

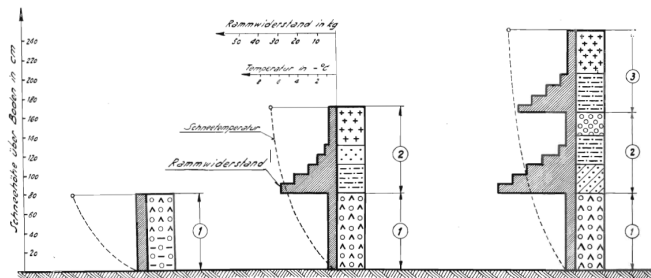


**Figure 2.2:** Snow-pack development by successive snow fall, Bucher (1948)

The first layer has a high-temperature gradient and little overweight. The second layer has a compaction zone in the lower part of its layer. The third layer will cause a loosening of the upper part of the second layer, as indicated by the change of crystals on the diagram. In summary, an interruption in the precipitations will generate differences in the plasticity and strength of the snowpack. The longer the time and the greater the temperature gradient between each precipitation, the larger the differences in properties will be. Thus, snow strength is greater in the lower part of each layer. This is a preliminary introduction to understanding how a layer and/or weak interface can form within a snowpack.

### Stresses and creeping in an inclined snowpack

As shown previously, a snowpack has different properties within it. Focusing on avalanche protection implies working with a snowpack on an inclined plane, with the specifications that this entails. The self-weight of the aggregates generates tensile, compressive, and shear stresses, causing deformation of the pack. Stress distribution and creep are defined by the velocity of each snow particle on a slope. The equations of the system will be detailed more fully in the next chapter 2.2.3 but Bucher's approach is expressed below: This expression of an inclined snowpack contains the following assumptions: constant weight, uniform strength, and plasticity.

Shear stresses are defined by:

$$\tau_x = \gamma_s \cdot \sin\psi \cdot (D - z) \quad [\text{Pa}] \quad (2.6)$$

The velocity along the x axis is given as:

$$v_x = \gamma_s \cdot \sin\psi \cdot a_3 \cdot \left(D \cdot z - \frac{z^2}{2}\right) \quad [\text{m/s}] \quad (2.7)$$

Where  $\psi$  is the angle of the slope, D is the thickness of the layer,  $a_3$  is defined constant and z is the desired depth for the calculation. These equations are presented only to highlight the dependency of density, slope angle, and snow depth on its lateral speed and shear stresses. As mentioned, Bucher (1948) formulation, and more common models will be discussed further.

### Creep damage

In these early works, creep is mainly defined as a consequence of in-homogeneity and obstacles on the slope (depression, ridge, etc.) and its damage process has been characterized as that of a semi-liquid, Bucher (1948). A draft guideline for the location of avalanche control structures is provided. It is very detailed and relevant at this early stage of snow engineering. It discusses surveying of the area, specifically wind directions, snow accumulation measurement over several winters, mass distribution along the slope, and geological conditions such as vegetation, soil type, and water concentration. In this perspective, an attempt to anticipate these creep pressures has been made.

### Creep pressure

A mass particle of length dx, height dz, and depth dy=1 is considered. The description of the compression and shear forces acting on the particle will not be detailed in this paper but can be found on page 63, Bucher (1948), although in German. From the definition of the velocities distributed on a wall along the x-axis,

$$v_x = -\gamma_s \cdot \sin\psi \cdot \frac{d^2}{2 \cdot \eta} \cdot \left[1 - \exp\left(-\frac{\pi \cdot x}{2 \cdot K_p \cdot d}\right)\right] \cdot \sin\left(\frac{\pi \cdot z}{2 \cdot d}\right) \quad [\text{m/s}] \quad (2.8)$$

It is possible to express the pressure distribution on the structure as a function of the depth z, by integrating the velocity with respect to x:

$$\sigma_s = -\gamma_s \cdot \sin\psi \cdot \frac{K_p \cdot \pi \cdot d}{4} \cdot \sin\left(\frac{\pi \cdot z}{2 \cdot d}\right) \quad [\text{Pa}] \quad (2.9)$$

Where  $K_p$  is a factor varying from 1.4 to 2 depending on the porosity and  $\sigma_s$  represents



the pressures normal to the structure.

To make the calculations more feasible in an engineering context, an integral of the stress on the surface of the wall has been done. The resultant  $S_1$  is applied in the upper part of the wall (around 2/3). The formula is given in the figure, 2.3. In this figure, the evolution of creep pressure in function of snow thickness and inclination is observable.

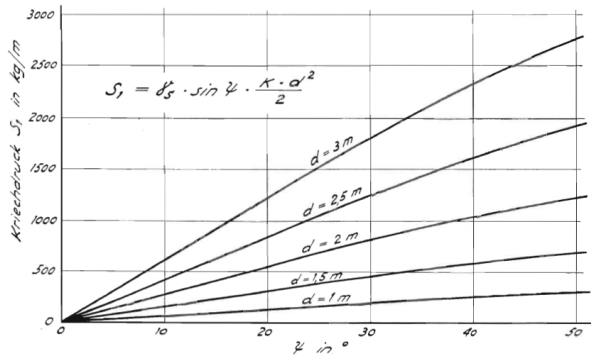


Fig. 65: Kriechdruck  $S_1$  in Funktion von Schneemächtigkeit  $d$  und Hangneigung  $\psi$   
(Für  $\gamma_s = 400 \text{ kg/m}^3$ ,  $K = 2$ )

**Figure 2.3:** Creep pressure  $S_1$  as a function of snow thickness,  $d$ , and slope angle,  $\psi$

This graph illustrates the influence of the slope angle and snow depth on the resulting pressure,  $S_1$ . It can be observed that for shallow snow depths, the value of the slope has little impact on the creep pressures. As soon as the snow depth increases, the pressure differences induced by slope variation are much greater.

This formulation allows the technical design of the snow support structure. It requires site studies and in-depth studies of snow properties, such as the behavior of snow density as a function of time.

The introduction of Bucher’s work made it possible to draw broad lines of snow mechanics at an early age and to show the global direction taken in the consideration of snow pressure on structures and creep. Extensive review work was carried out and provided a good overview of the status of snow mechanics in the late 1970s.

## 2.2.2 Reviewing work - Mellor

As stated in the introduction [1], Mellor (1975), Salm (1977) have done an impressive job of reviewing the current state of snow mechanics. Since their work, the basis of snow mechanics has not changed fundamentally. The democratization of finite element analysis

has allowed advanced analytical research, mainly including parametrization. This is particularly seen in the work on the 2D equation of creep pressures.

Mellor (1975) has focused on the basic definition of snow mechanics. With this work, the assumptions necessary for further analysis will be taken up, as well as the deformation and rheology model. There, snow is defined as a quasi-homogeneous sintered compact material composed of equal ice grains. The definition of the model moves from elastoplastic to viscoplastic. The viscoplasticity allows for defining irreversible and time-dependent deformations, which was missing in the elastoplastic model. Snow's behavior is better defined by viscoelastic and temperature-sensitive model. In the case of failure, snow exhibits three types of failure: viscoplastic failure, brittle failure, and transitional failure. The triggering mechanisms play an important and interesting role in the study of avalanches but are a separate topic and will not be discussed in this thesis.

A major disparity compared to the behavior of ice, is the high porosity of snow, leading to high irreversible compressibility. The rheological description is still a field of research and simplifications are needed for application in engineering.

### Deformation model

In an idealized case of non-destructive loading, Burgers model is the most widely used to describe viscoelastic deformations. This model consists of two units in series, the Maxwell and Kelvin-Voigt models. Maxwell's model puts in series a spring (elastic response) and a dash-pot (viscous response). This model is used to describe stress relaxation but not creep. This is the reason why the Kelvin-Voigt unit is added: to model the creeping process, where the spring and the dash-pot are put in parallel, see figure 2.4

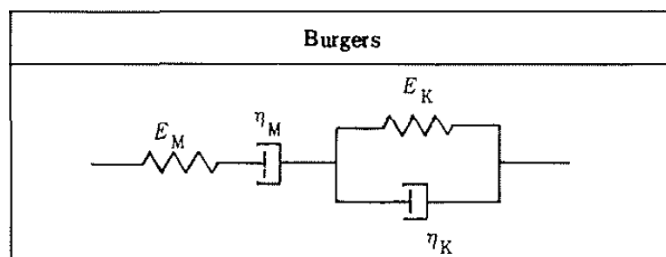


**Figure 2.4:** Burger's model from Mellor (1975)

The general equation for the Burger model response is given as follows in Mellor (1975):

$$\ddot{\sigma} + \left( \frac{E_M}{\eta_M} + \frac{E_M}{\eta_K} + \frac{E_K}{\eta_K} \right) \cdot \dot{\sigma} + \frac{E_M \cdot E_K}{\eta_M \cdot \eta_K} \cdot \sigma = E_M \ddot{\epsilon} + \frac{E_M \cdot E_K}{\eta_K} \cdot \dot{\epsilon} \quad (2.10)$$

Where M and K indices correspond to Maxwell and Kelvin-Voight unit, Young's modulus is E,  $\eta$  correspond to viscosity, stress and strain are, respectively, noted  $\sigma$  and  $\epsilon$  and are derived against the time, t.

There are simplifications for the special cases of constant stress,  $\sigma_0 = constant$  and constant strain rate,  $\dot{\epsilon} = constant$ . They can be found in Mellor (1975), page 254 and 256. Burger model is good for describing the deviatoric deformation of the material, but without accounting for bulk stresses (no change in volume). Therefore, it places the snow-pack deformation in a pure shear context: elongation of the material in one direction and shortening in the perpendicular direction.

The rheology of the snow is described by the classical Young's modulus, E, shear modulus, G, bulk modulus, K, and Lamé coefficient,  $\lambda$ . Determining the visco-elastic properties seems relatively doable, by an interpretation of the creep curves in a constant stress test in pure shear stress setting. However, it appears that when bulk stresses cannot be avoided, which happens in reality, the determination of the rheology coefficient becomes quite tricky.

If we focus on the study of creep, a new description of the relaxation time is presented, no longer involving the shear modulus but Young's modulus. Relaxation time is now defined by the ratio  $\frac{E_K}{\eta_K}$  in the Kelvin-Voigt unit.

### 2.2.3 Reviewing work - Salm

Salm (1977) reviewed the formulations of snow pressure on a structure made by various scientists before 1977. He included a focus on engineering expressions of these pressures in his paper, where he has compiled several formulations of the pressure on a wall. The following section will present each of the equations, along with their assumptions and range of validity. A common hypothesis of these models is to consider snow as a Newtonian fluid, which means that the viscosity is kept independent from stresses. In reality, slowly moving snow is assumed to be a non-Newtonian fluid whose Newtonian behavior is accepted only within a limited range of low stresses, Salm (1977).

The concept of a neutral zone has to be introduced. It consists of a snow-pack area where all gradients parallel to the ground have disappeared. These gradients include

boundary conditions, snow characteristics, slope angle, and snowpack thickness. It represents the area of validity for all following models. The majority of them were not proven at the boundaries, ground, and air. If the model has a larger area of validity, it will be specified in the description of the models.

The formulation of Haefeli's theory is discussed first and in more detail, as it lays the foundation for all subsequent researcher work.

### Haefeli's model

An inclined snow cover with constant density and Newtonian fluid, i.e. linear relation between stresses and rate of deformation, is considered. The two boundary conditions are a surface free of stress and a zero settlement rate on the ground. Taking into account a local coordinate system (axis  $x$  parallel to the slope and  $y$ -axis perpendicular to it) stresses in this system are expressed in function of slope angle,  $\phi$ , density,  $\gamma$ , and the viscous analog of the cross-section number,  $m$ . The equations of the system are valid in the "neutral zone":

$$\sigma_x = -\gamma x \cos \psi \quad [\text{Pa}] \quad (2.11)$$

$$\tau(xy) = -\gamma x \sin \psi \quad [\text{Pa}] \quad (2.12)$$

$$\sigma_y = \sigma_z = \frac{\sigma_x}{m - 1} \quad [\text{Pa}] \quad (2.13)$$

$$\tau(yz) = \tau(xz) = 0 \quad [\text{Pa}] \quad (2.14)$$

The parameter 'm' is also explained as "ratio of the longitudinal to the lateral rate of deformation in the uni-axial state of stress.", Salm (1977).

In later formulations, the concept of the viscous analog,  $m$ , is replaced and adapted in the equation, by the more easily understandable Poisson's ratio,  $\nu$ . It is possible to deduce the velocity in both directions, respectively  $x$  and  $y$ :

$$u = u_0 \left(1 - \frac{x^2}{D^2}\right) \quad [\text{m/s}] \quad (2.15)$$

$$v = v_0 \left(1 - \frac{x^2}{D^2}\right) + v_g \quad [\text{m/s}] \quad (2.16)$$

Where  $D$  is the snow thickness, i.e. snow height perpendicular to the slope,  $u_0$  and  $v_0$  are the speed at  $x = 0$ , and  $v_g$  is the gliding velocity.

Haefeli et al. (1939) introduces a concept of creep angle,  $\beta$ , which is the angle between the two velocity vectors,  $u$  and  $v$ , of a particle in the neutral zone without considering

gliding and in the ground-parallel direction, recalled by Salm (1977)

A large part of this ratio is attributed to pressures generated by the interruption of gliding and creep by a wall. While the creep process has already been mentioned, gliding has to be defined. It is the movement of the entire snowpack over the ground, it requires a wet interface i.e. at a temperature  $\geq 0^\circ C$ . Gliding has been well studied by Haefeli (1948). It came to introduce the term glide velocity,  $v_g$ , and relative glide velocity,  $n$ :

$$n = \frac{v_g}{v_0} \quad [-] \quad (2.17)$$

Glide parameter is after empirically determined by:

$$N = \sqrt{1 + 3n} \quad [-] \quad (2.18)$$

This empirical glide equation, based on field test data, will be used in the Swiss Guidelines (2007) but defined by slope exposure and soil roughness.

In order to have a more realistic approach in assessing pressures, Haefeli et al. (1939) defined a zone called back-pressure,  $y_b$ , that corresponds to the effective range of snow support structure in a slope. This zone is intended to counteract the simplistic assumption that the snowpack is a homogeneous block of snow, which induced an increasing pressure with distance from the slope.

$$y_b = -H \cdot \sqrt{\frac{2}{\tan\beta_{45^\circ}}(1 + 3n)} \quad [\text{m}] \quad (2.19)$$

$\tan\beta_{45^\circ C}$  is approximated to 0.32 by Haefeli et al. (1939):

$$y_b \approx -2.5 \cdot H \cdot N \quad [\text{Haefeli } 48] \quad [\text{m}] \quad (2.20)$$

$H$  is the snow height, i.e. the vertical height of snow in the snow-pack:  $H = D \cdot \cos(\psi)$

Haefeli (1948) provided a final formulation of the distributed load of the snow pressure on the wall, therefore  $S'_N$  is considered per unit of length across the slope:

$$S'_N = \frac{\gamma}{2} \cdot H^2 \left[ (1 - 2 \cdot \tan\beta_{45^\circ} \cdot \cos^3\psi + \frac{1}{3} \sqrt{\frac{2}{\tan\beta_{45^\circ}}} \cdot \sin 2\psi \cdot \sqrt{1 + 3n}) \right] [\text{Pa}] \quad (2.21)$$

### **Bucher's model**

Similarly, Bucher (1948) formulated equations for snow pressure on a wall. He also assumed Newtonian behavior but did not include gliding. He made hypotheses about the boundaries conditions, which led to the applicability of the model only for low-density

snow and an inaccurate definition of tangential force near the surface, Salm (1977). This results in a definition of the back-pressure zone,  $y_b$

$$y_b = -\frac{6}{\pi} D \cdot \sqrt{\frac{2m}{m-1}} \quad [\text{m}] \quad (2.22)$$

Stresses normal to the wall,  $S'_N$

$$S'_N = -\frac{\gamma}{2} \sin\psi \cdot D^2 \cdot \sqrt{\frac{2m}{m-1}} \quad [\text{Pa}] \quad (2.23)$$

### Ziegler's model

Ziegler decided to apply plasticity theory to snow mechanics to describe creeping processes. He was motivated by the fact that studies of Haefeli (1948) and De Quervain (1945) showed that slow and irreversible deformations serve to describe snow as a viscoelastic material and could therefore be characterized by plasticity theory under certain simplifications. To apply his theory, he made the following assumptions, homogeneity, and incompressibility of the snow. While homogeneity can be adapted to various snowpack cases, incompressibility considerably reduces the applicability of the formulated equation. Normal stresses, on the wall, are expressed in the paper Ziegler (1963), for a study case of an inclined infinitely long layer, which consists of the rigid-ideal plastic material. The formula has been harmonized with the notation used in the Salm paper,

$$\sigma_y = -k \cdot \left[ \frac{x}{D} \cot\psi + 2 \cdot \sqrt{1 - \frac{x^2}{D^2}} \right] \quad [\text{Pa}] \quad (2.24)$$

And the resultant  $S'_N$  is define as,

$$S'_N = -k \cdot \frac{D}{2} \cdot (\cot\psi + \pi) \quad [\text{Pa}] \quad (2.25)$$

Whereas  $k$  is the shear yield strength, it is defined with the critical thickness where slip occurs:

$$D_{er} = \frac{k}{\gamma \sin\psi} \quad [\text{m}] \quad (2.26)$$

Ziegler (1975) also consider an critical distance,  $L_{er}$ , which is the distance, not to be exceeded, between two barriers in slope. This distance can be assimilated to the back-pressure zone,  $y_b$  mentioned above.

$$L_{er} = y_b = \frac{k}{\gamma} \cdot \frac{\cot\psi + 3\pi}{2\sin\psi} \quad [\text{m}] \quad (2.27)$$

### McClung's model

Since the late 1970s, McClung's work has contributed greatly to a better understanding of snow mechanics from creep process to slab failure. In 1982, he tackled the problem of the 1-D definition of snow pressures on a structure on a slope. McClung (1982) introduce a clearer notation when he chose to work with Poisson's coefficient,  $\nu$  instead of the difficult-to-represent parameter "m".

Poisson's ratio enables the characterization of the contraction of mass perpendicular to the direction of the effort applied. The writing and the dependence of the creep on the Poisson's ratio are used in all the works that followed in the 90s and 2000s.

A schema, found in McClung (1982), states well the basic parameters and coordinate system used, see fig. 2.5:

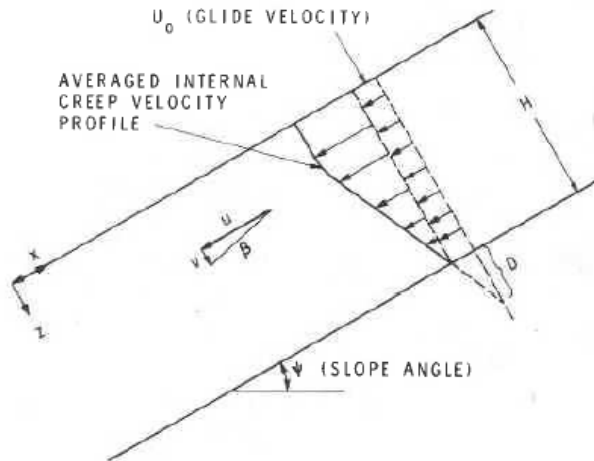


FIG. 1. Definition of coordinate system, stagnation depth,  $D$ , creep angle,  $\beta$ , and creep velocity components ( $u, v$ );  $U_0$  is the glide velocity and  $\psi$  is the slope angle.

Figure 2.5: Definition of velocities inside the snowpack

McClung expresses the creep angle as a function of the slope and the Poisson's ratio and is represented in the figure. 2.5. This definition is derived from the deformation coefficient in the neutral zone,  $C_D$ , from the generalization work of Perla (1972). This coefficient corresponds to the ratio of the strain rate of both creep components,

$$C_D = -\frac{\frac{\partial v}{\partial z}}{\frac{\partial u}{\partial z}} = \frac{1}{2} \cdot \left( \frac{1 - 2\nu}{1 - \nu} \right) \cdot \cot\psi \quad [-] \quad (2.28)$$

As long as the area studied is far from the boundaries,  $C_D$  is equalized to the tangent of creep angle,  $\tan\beta$ , therefore:

$$\tan\beta = \frac{1}{2} \cdot \left( \frac{1 - 2\nu}{1 - \nu} \right) \cdot \cot\psi \quad [-] \quad (2.29)$$

The geometric component  $D^*$  (seen as  $D$  in figure. 2.5) is a function of the Poisson's ratio and the geometry of the interface at the boundary, states McClung (1982). In practice, its value is determined geometrically, by knowing the values of the creep and glide velocity. In figure. 2.5, the principle of geometrical determination of  $D^*$  is shown. The boundary conditions of  $D^*$  are, no glide ( $D^*=0$ ) and no drag ( $D^*$  is then infinite).

McClung developed a first equation for stress normal to the wall,  $\bar{\sigma}_x$  in 1982. He specified it in 1989 in the paper made in collaboration, McClung and Larsen (1989). This paper also goes into more detail about boundary conditions of the snowpack. They state two extreme cases of boundary conditions on the wall. The first, traction free, represents the case of a smooth interface between the structure and the snow, with the presence of water. This means that the shear stress,  $\tau_{xz}$ , is zero. The second condition, no-slip, corresponds to zero creep velocities,  $u$  and  $v$ , at the contact of the structure and no free water at the interface, and therefore entails the presence of shear stress along the wall surface. The real boundary condition is an intermediate between these two extreme cases and also closer to the no-slip condition say McClung and Larsen (1989) but has not been studied by them. The complexity of the modeling of the no-slip condition leads to errors of the order of 10% when calculating the normal stresses, McClung and Larsen (1989).

For these reasons, its formulation is not introduced and the focus will be on the traction-free condition. From McClung (1982)'s expression, boundary condition influenced the two parameters  $\bar{\sigma}_z(0)$  and  $\frac{L}{H}$ . Since there is no shear along with the structure, creep velocity in the  $x$ -direction,  $u$ , is null and the normal stress has a rectangular form along the structure and the depth average is written as follows,

$$\bar{\sigma}_z(0) \approx \frac{1}{2} \rho g H \cos\psi \quad [\text{Pa}] \quad (2.30)$$

The dimensionless creep parameter,  $L/H$ , depends on the Poisson's ratio. Its dependence on  $\nu$  has been formulated empirically after many sets of finite element calculations, made by McClung and Larsen (1989). This formulation is valid for the boundary condition, traction-free:

$$\frac{L}{H} = 0.27 + \frac{\nu}{12} \quad [-] \quad (2.31)$$

The final depth-average stress at the wall is presented below, from McClung and Larsen



(1989). The equation is valid in the following ranges, McClung (1982):  $25^\circ \leq \psi \leq 55^\circ$ ,  $0 \leq \nu \leq 0.4$  and  $0 \leq \frac{D^*}{H} \leq 3$

$$\bar{\sigma}_x(0) = \bar{\rho}gH \cdot \sin\psi \cdot \left[ \left( \frac{2}{1-\nu} \right) \left( \frac{L}{H} + \frac{D^*}{H} \right) \right] + \bar{\rho}g \frac{H}{2} \cdot \left( \frac{\nu}{1-\nu} \right) \cos\psi \quad [\text{Pa}] \quad (2.32)$$

## 2.2.4 Parametrization of Temperature - Teufelsbauer

In recent years, Teufelsbauer (2011) wanted to model the viscosity of snow for a wider range of snow density and temperature. For this, he relied on existing models and two data sets of De Quervain (1945) and Abe (2001). These two experiments are presented in the following section, 2.4. Following the work of Bartelt et al. (2000) et al and a new understanding of snow behavior in recent years, the main factor controlling creep is defined as the viscosity of the snow. Viscosity is then described as a function of snow density and temperature.

An overview of existing models was made by Teufelsbauer, who collected 6 different models. These models all include an exponential function. However, three of them do not include temperature and were therefore discarded, as they are not designed to model a wide range of temperatures. This temperature gradient is more and more often encountered in the Alps, as well as in the Arctic in recent years, and needs to be accounted for. A fourth one was rejected because it did not reproduce the existing results.

The models of Abe (2001) and Gubler (1994) are retained:

$$\eta_{Abe} = 0.21 \cdot e^{-0.166T} \cdot \rho^{4.0} \quad [\text{Pa/s}] \quad (2.33)$$

$$\eta_{Gubler} = 1.85 \cdot 10^{-6} \cdot e^{0.02\rho+8100/(T+273.5)} \quad [\text{Pa/s}] \quad (2.34)$$

The first one provides too low viscosity for high snow density while the second one gives too high viscosity for low snow density. Therefore, Teufelsbauer presented a new model, combining both the good performance of Abe's model for low density and Gubler's model for high density:

$$\eta_s = 0.05 \cdot \rho^{-0.0371 \cdot T + 4.4} (10^{-4} \cdot \exp(0.018 \cdot \rho) + 1) \quad [\text{Pa/s}] \quad (2.35)$$

Where,  $\nu_s$  is compactive viscosity, representing the compressibility of the snowpack,  $T[^\circ\text{C}]$ , snow temperature and  $\rho [kg/m^3]$  snow density.

Teufelsbauer also tackles the formulation of Poisson's ratio as a function of snow density and temperature. The importance of Poisson's ratio is critical in some formulation of snow pressures on a wall, as shown by McClung, in 2.2.3. It is also directly connected to compactive viscosity through viscosity, Gubler (1994). Varying it as a function of snowpack properties allows for greater accuracy than using a constant,  $\nu$ . Based on Mellor's work, and in-situ data, an empirical method was formulated to qualify  $\nu(\rho, T)$ :

$$\nu(\rho, T) = \nu_{max} \cdot \frac{\bar{\nu}(\rho, T) - \bar{\nu}(0, T)}{\bar{\nu}(1000, T) - \bar{\nu}(0, T)} \quad [-] \quad (2.36)$$

$\bar{\nu}(\rho, T)$  is written,

$$\bar{\nu}(\rho, T) = a \tan\left(\frac{\rho - \rho_p(T)}{r_\rho}\right) \quad (2.37)$$

and  $\rho_p(T)$ ,

$$\rho_p(T) = \rho_p^0 - r_T T \quad (2.38)$$

Where  $\nu_{max} = 0.49$  is define as the maximal  $\nu$  reachable,  $r_T = 15$  and  $r_\rho$  are constant corresponding to the influence of snow temperature and snow density,  $\rho_p(T)$  represents the density where  $\nu(\rho, T)$  change curvature, and  $\rho_p^0 = 300 [kg/m^3]$  stands for the density at the upper boundary where  $T = 0^\circ C$ .

This formulation allows the determination of the Poisson's ratio only based on the density and temperature of the snowpack. In this way, variations in snowpack properties are taken into account in the pressure calculations. However, in reality, these two data, especially the density, are difficult to obtain throughout the season and show great variability.

## 2.3 Poisson's ratio

Poisson's ratio has been introduced in 2.2.4 section and plays an important role in the determination of lateral pressure of snow. From the literature, several studies have tackled the evaluation of this parameter, Larsen et al. (1985), Larsen (2000), Abe (2001), Teufelsbauer (2011), Navarre et al. (2007), etc. The parameters are often given with a density range and/or information on the method of determining the factor.

<u>Paper</u>	<u>Poisson's ratio</u>	<u>Comments</u>
<b>Abe (2001)</b>	0.27	Light artificial snow
<b>Larsen et al. (1985)</b>	0.25	
<b>Bader and Salm (1990)</b>	0.2	Express as m inverse of $\nu$ in literature
<b>Larsen (2000)</b>	0.36	Maritime environment
<b>Schweizer (1999)</b>	0.2	
<b>Navarre et al. (2007)</b>	0.25	$\rho = 400-600 \text{ kg/m}^3$

**Table 2.1:** Poisson's coefficient formulate in the literature

Teufelsbauer (2011) analyzed data from previous research on the viscous Poisson's ratio. Papers included work from Bader H (1951), R (1966), M (1966), Yoshida (1963) and McClung (1975). Viscous Poisson ratio is plotted in figure 2.6 in function of the density. From these data, Teufelsbauer has developed the formulation expressed in 2.36. Two conditions are imposed on the temperature to represent the maximum and minimum cases and show a data envelope. Upper limit is set at  $T = 0^\circ$ , while the lower limit at  $T = -16^\circ$ .

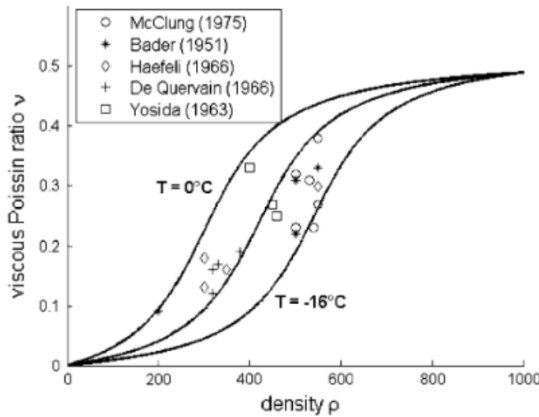


**Figure 2.6:** Viscous analogue envelope, Teufelsbauer (2011)

When the site characteristics are studied in the section 5, a definition of the Poisson coefficient will be presented taking into account the density and temperature of the snow relative to our site.

## 2.4 Laboratory experiments - Two approaches

Laboratory studies of snow creep have been rather rare in recent years. Although De Quervain was interested in settlement and compaction of the snow at an early stage, few studies have followed up. The reason given was the complexity of reproducing the settings in-situ in the laboratory. Therefore, there is a lack of data to run and validate models. One of the experiments on artificial snow was made by Abe (2001). These two experiments are presented below, together with the conclusions that were drawn at the time.

### 2.4.1 De Quervain

One of the first experiments was conducted by De Quervain (1945). At that time, De Quervain was more interested in the long-term settlement of snow. The experiment consisted of snow samples of the same density ( $115\text{kg}/\text{m}^3$ ) placed in wooden boxes subjected to different temperatures (from  $-2^\circ\text{C}$  to  $-32.5^\circ\text{C}$ ). Then, the samples are left alone for one hundred days. It appears that the maximum density was reached for lower temperatures,  $300\text{kg}/\text{m}^3$  for  $-2^\circ\text{C}$  against  $130\text{kg}/\text{m}^3$  at  $-32.5^\circ\text{C}$ . This experiment illustrated the relationship between temperature and snow density. A difference of  $32.5^\circ\text{C}$  in ambient temperature resulted in a 56% difference in density after 100 days. These data were used by Teufelsbauer (2011) to calibrate his viscosity model.

### 2.4.2 Abe

A Japanese study, led by Abe (2001), studied creep behavior in the laboratory. The research focused on experimentally creating low-density snow ( $< 100\frac{\text{kg}}{\text{m}^3}$ ). The snow layer is placed on a frozen table, to neglect gliding, and then left to rest for a few hours. Afterward, the table is tilted to the desired angle. Tests are performed at different temperatures. The deformations are monitored over time using chopsticks and blue ink. The calculation assumptions are the plain strain theory, constant Poisson ratio, and a linear viscous law. Once the table is tilted, the layer is left to flow for three days. Two tests have been made at  $-19.5^\circ\text{C}$  and  $-11^\circ\text{C}$ . The results for the temperature  $-11^\circ\text{C}$  are shown in the figure, 2.7:

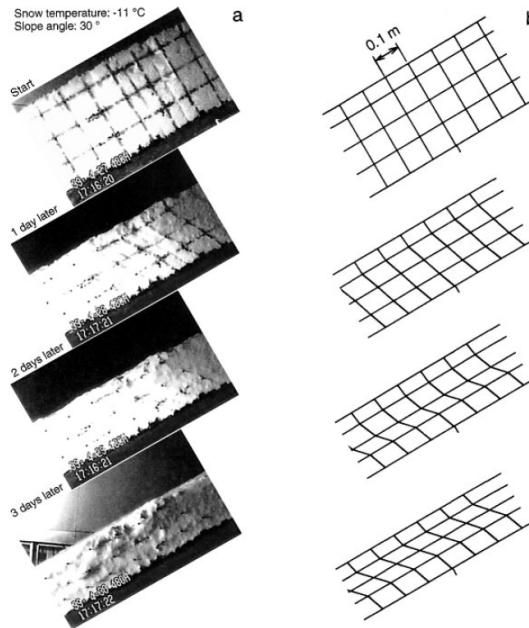


Fig. 6. Comparison of the deformation between experimental (a) and computed (b) results at a snow temperature of  $-11^{\circ}\text{C}$ .

**Figure 2.7:** Creep measurements during Abe’s experience on the left and computed results on the right

After comparing the two temperature results, it appears that the highest temperature generated more deformation in the parallel and perpendicular directions of the slope. It is coherent with the understanding of how temperature plays a role in the deformation of a snowpack.

## 2.5 Swiss guidelines

The Swiss Guidelines (2007) are considered the standard for the construction of avalanche defense structures by the vast majority of engineers. The Swiss practice standards were first published in 1961. B. Salm and R. Haefeli mainly contributed to the publication. The standards have been revised three times to include new anchoring techniques and safety factors, in 1968, 1990, and 2007 by Margreth (2016). This latest updated version has been translated into many languages, including English, French and Italian, to extend its use to most countries.

These guidelines cover in detail all the steps needed during the construction of snow support structures. The standard discusses the factors influencing the positioning of avalanche

control structures, such as the triggering of mechanisms, type of structures, snow height, the role of the distance between constructions, etc.

Special attention is given to the definition of snow pressures, including consideration of creep and gliding factors and the accentuation of forces at the edges of the features. Based on the formulation of pressures, guidance is given on the structural design of structures. A section is devoted to the anchoring of structures in permafrost, alpine in this case, whose extension to the Arctic case is possible but subject to discussion.

We will look in more detail at the definition of pressures made for engineering purposes. The aim was to formulate an equation that is easy to understand and use but still represents reality. The concern is also to overestimate the pressures and thus increase the costs for construction and implementation.

### Planning of structures

The purpose of snow support structures is to prevent the triggering of avalanches and their function is to resist creep and sliding movements, Swiss Guidelines (2007)

When planning the construction of structures, there are several parameters to assess, according to the Swiss guidelines. Most of the avalanches' dangers considered by the structure are coming from slab avalanches. Therefore, knowing the controlling factors of these avalanches and snow behavior are necessary to have efficient protection equipment. Swiss Guidelines (2007) outline 4 parameters influencing creep and glide of snowpack: slope angle, thickness, ground roughness, and snow characteristics (deformability, friction, etc.)

In essence, the first row of structures should be positioned below the highest observed fracture line, or as close to the toe of a cornice as possible in this case. Fence rows should stop when the slope drops below 30° or when it is deemed that avalanches are no longer having a dangerous impact.

### Snow Height

Snow height is one of the determining parameters for the design of structures. A concept of extreme snow height, for the site, is introduced and the height of the structure must be greater than or equal to this,

$$H_{extreme} = H_{max} \cdot \frac{\bar{H}_{extreme}}{\bar{H}_{max}} \leq H_{structure} \quad [\text{m}] \quad (2.39)$$

Where  $H_{max}$  is the maximal snow height measured at the site,  $\bar{H}_{max}$  is averaged for an area around the site and  $\bar{H}_{extreme}$  is the extreme snow height averaged over the area,

which depends on elevation and security factor for area.

**Snow pressures: definition and dimensioning**

Pressure parallel to the slope,  $S'_N$ , are expressed as following:

$$S'_N = \rho \cdot g \cdot \frac{H^2}{2} \cdot K \cdot N \quad [\text{kN/m}] \quad (2.40)$$

Where  $H$  is the vertical snow height,  $K$  &  $N$  are, respectively, creep and glide factors. It can be observed that the snow pressure does not depend on the depth and is therefore constant along with the structures. The purpose of this assumption is to simplify the calculations and equations for engineering.

The creep factor is presented, in the literature, as dependent on the slope angle and snow density, see the table below, 2.2:

$\rho [t/m^3]$	0.2	0.3	0.4	0.5	0.6
$K/\sin(2\psi)$	0.7	0.76	0.83	0.92	1.05

**Table 2.2:** Creep factor definition from Swiss Guidelines (2007)

Glide factor is dependent on the slope exposure and ground roughness and is found in fig.2.8:

Ground classes	Glide factor	
	Exposure WNW-N-ENE	Exposure ENE-S-WNW
<p><b>Class 1</b></p> <ul style="list-style-type: none"> <li>• Coarse scree (<math>d^* \geq 30</math> cm)</li> <li>• Terrain heavily populated with smaller and larger boulders</li> </ul>	1.2	1.3
<p><b>Class 2</b></p> <ul style="list-style-type: none"> <li>• Areas covered with larger alder bushes or dwarf pine at least 1 m in height</li> <li>• Prominent mounds covered with grass and low bushes (height of mounds over 50 cm)</li> <li>• Prominent cow trails</li> <li>• Coarse scree (<math>d^*</math> ca. 10–30 cm)</li> </ul>	1.6	1.8
<p><b>Class 3</b></p> <ul style="list-style-type: none"> <li>• Short grass interspersed with low bushes (heather, rhododendron, bilberry, alder bushes and dwarf pine below approx. 1 m in height)</li> <li>• Fine scree (<math>d^* \leq 10</math> cm) alternating with grass and low bushes</li> <li>• Smallish mounds of up to 50 cm in height covered with grass and low bushes, and also those alternating with smooth grass and low bushes</li> <li>• Grass with shallow cow trails</li> </ul>	2.0	2.4
<p><b>Class 4</b></p> <ul style="list-style-type: none"> <li>• Smooth, long-bladed, compact grass cover</li> <li>• Smooth outcropping rock plates with stratification planes parallel to the slope</li> <li>• Smooth scree mixed with earth</li> <li>• Swampy depressions</li> </ul>	2.6	3.2

$d^*$  is the boulder diameter characteristic of the roughness of the ground surface.

**Figure 2.8:** Table containing glide factor for different ground roughness and slope exposure, Swiss Guidelines (2007)

Normal component of the pressure is expressed as follows,

$$S'_Q = S'_N \cdot \frac{a}{N \cdot \tan\psi} \quad [\text{kN/m}] \quad (2.41)$$

This formulation has first been made by Haefeli (1948) to pass from normal to tangent pressure. The coefficient "a" varies from 0.2 (dense) to 0.5 (loose) according to the type of snow present and is specified by field tests according to Haefeli (1948).

If the fence is not perpendicular to the slope, the weight of the snow prism created needs to be added to both of the components of the snow pressures. This weight depends on the deviation angle from 90°, snow density, gravitational acceleration, and snow thickness.

The final design consideration is to verify that the design snow pressure is less than or equal to the design resistance of the structure. The snow load,  $Q_k$  is accounted as variable action, therefore needs to be factorized by a safety factor,  $\gamma_Q$ , is equal to 1.5, according to Eurocode. The strength of the structure is determined by a ratio of the profile strength of the material,  $R_k$  (e.g. steel) to a safety factor,  $\gamma_M$ , that takes into account the use and position of the section under consideration.

$$E_d = \gamma_Q \cdot Q_k \leq \frac{R_k}{\gamma_M} \quad [\text{kN/m}] \quad (2.42)$$

Lateral snow pressure distribution is not uniform. Pressures on the side of the structure are increased by the flowing of the snow around them. At this position, creeping is much larger than against the center of the structure. This effect can be considerable and much more than double the initial normal pressure on the center of the structure. In the guideline, it is defined as a coefficient,  $f_R$  that is multiplied with  $S'_N$ . It is dependent on the lateral distance between two structures but it is also limited by a function of the gliding,  $N$ .

$$f_R = (0.92 + 0.65 \cdot N) \cdot \frac{A}{2} \leq (1.00 + 1.25 \cdot N) \quad [-] \quad (2.43)$$

Where  $A$  is the lateral distance between two structures The horizontal length affected by this effect is controlled by  $A$ , or the effective height of the support,  $D_k = H_k \cdot \cos(\psi)$ .  $H_k$  is the vertical structure height.

$$\Delta l = 0.60 \cdot \frac{A}{2} \leq \frac{D_k}{3} \quad [\text{m}] \quad (2.44)$$



## 2.6 Norwegian standards

Based on pressure data collected by the Norwegian Geotechnical Institute (NGI) in the seventies and eighties, detailed in the next section 2.7.1. Larsen (2000) proposed a design coefficient for snowpack exposed to maritime climate. It builds on the previous pressure formulation made in collaboration, McClung and Larsen (1989), written in equation 2.32. He estimates the safety factor at 1.5 for the central part of the structure:

$$\sigma_m = 1.5 \cdot \bar{\sigma}_x \quad [\text{Pa}] \quad (2.45)$$

And in order to take the end-effect in account,

$$\bar{\sigma}_r = 2.8 \cdot \bar{\sigma}_x \quad [\text{Pa}] \quad (2.46)$$

Norwegian public research has published some guidelines regarding avalanches and road construction, and protection. Through the work of Norem (2014), an equation of the snow pressure on structure in a slope is proposed. This equation is empirical and based on Larsen (2000) paper. This equation is made for engineering purposes in Norway, therefore it includes directly the safety factor for the maritime environment. Poisson ratio is replaced by an empirical value of  $\nu = 0.36$ , defined in Larsen et al. (1985). Consequently, a rewrite of equation 2.32 for engineering design is,

$$\sigma_x = \rho g h \cdot [3.125 \cdot \sqrt{0.25 \cdot \sqrt{\sin\psi} + 0.05 \cdot \sin\psi} + 0.28 \cdot \cos\psi] \quad [\text{Pa}] \quad (2.47)$$

## 2.7 Case-Studies - In-situ data collection

To conclude this section, two case studies of in-situ experiments on snow pressure on structures are introduced. Two groups of researchers have done detailed work on structural supports, Larsen et al. (1985) in Grasdalen, Norway and Hewes et al. (2016) in Wyoming, USA.

Both experiments have a similar set-up, the objective was to monitor snow support structures with pressure cells on the retaining surface and strain gauge positioned on the steel frame, in the eighties for McClung & Larsen and thirty years later for Hewes et al.

### 2.7.1 McClung & Larsen - Norway

The test site is located in western Norway, at Grasdalen. The structure is positioned in a 25° slope at 1170m elevation and is 3.4m high. Because of its location, close to a maritime

environment, and exposed to strong winds, it is prone to exhibit wind-packed snow which is, in general, stiffer than that of the Alps. The monitoring devices are placed in the center of the structure to avoid end-effect and shear stresses in the data. These effects are not negligible but were complicated to incorporate into the model at this stage of the theory. The monitored structure includes pressure cells on the part holding the snowpack and deformation gauges on the metal structure of the support, see fig. 2.10:

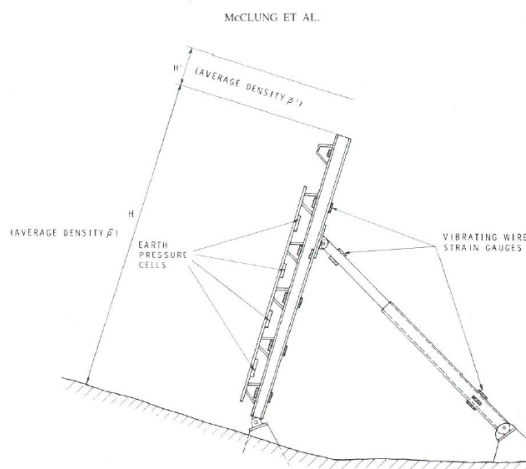


**Figure 2.9:** Schema of the monitored structure from Larsen et al. (1985)

According to Larsen et al. (1985), the pressure cell method is only effective in the case of a dry snowpack and then used as a validation of the back-calculated pressures by the strain gauge. Strain gauges have proven to be a successful method even in wet snow-pack but require a minimum pressure to be detected in the very rigid metal structure. Its errors have been estimated to a maximal of 10%. Pressure distribution found by back-calculation of strain gauge is presented in fig. 2.10:

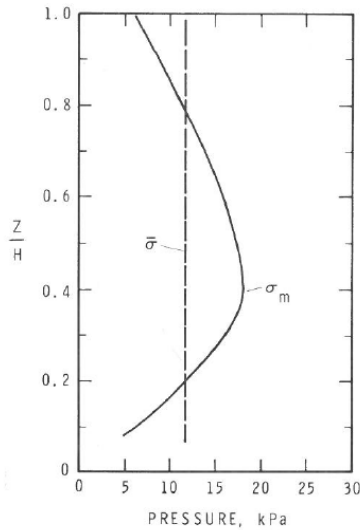


**Figure 2.10:** Pressure distribution over the structure from strain gauge data - maximal pressure,  $\sigma_m$  and mean pressure,  $\bar{\sigma}$ , are represented

Pressure distribution has a parabolic shape with the maximal pressure arising below the mid-height, approximately  $0.4 \cdot H$ . Pressures are not null at the top of the support because the snow height overcame the structure height. Maximum pressures are calculated to be around 18 Pa. While the depth-averaged snow pressures are estimated at around 12 Pa. The density of hard, wind-packed snow can be assumed to be about  $500 \frac{kg}{m^3}$ , which leads to a resting pressure of about 10 Pa at 2 m depth ( $0.4 \cdot H$ ) and leaves much of the built-up pressure to active snowpack movements such as creep and glide.

The conclusions of the extensive data processing work, published by Larsen (2000), is used for the development of Norwegian standards, seen in section 2.6. Larsen has made conclusions on critical parameters definition for the specific case of Norwegian maritime-influenced snow-pack. He established that elevation and exposure have low to no impact on snow-pack pressures difference. According to him, no glide has been observed at the site. Design value for density is  $500 \frac{kg}{m^3}$ , while average being  $459 \frac{kg}{m^3}$  with a standard deviation of  $48 \frac{kg}{m^3}$ . The fitted Poisson coefficient for the data was found to be  $\nu$  equal to 0.36, for this maritime snow-pack. He also noted that maximum pressures were often encountered at mid-height, corresponding, on average, to 1.43 times the average pressure.

## 2.7.2 Wyoming

In 2005, on an initiative of the transportation department of Wyoming, snow supporting structures are been considered on a slope above Milepost 151 road. This technique was completely new to the US, while it has been shown that it has been used extensively in Europe in the past decades. The project was guided by the release of Swiss Guidelines (2007) in the English language in 2007. The objective is to monitor structures in the same way as Larsen et al. (1985) and adapt the alpine-based guidelines to North America's snowpack particularities. The site is characterized by a 35° south-west facing slope at roughly 2200m elevation. The glide factor has been set to  $N = 3.0$  due to the low roughness of the ground and south exposition. Using the very conservative formula in Swiss guidelines, snow pressure parallel to slope is calculated:

$$S_N = 64 \cdot H^2 \cdot N \cdot f_R \quad [\text{kN/m}] \quad (2.48)$$

End-effect has also been assessed using Swiss Guidelines. It has been assumed that  $N = 3.0$  and the distance between fences,  $A$ , infinite. Then  $f_R$  is formulated as:

$$f_R = (1.00 + 1.25 \cdot N) = 4.75 \quad [-] \quad (2.49)$$

The structure is 1.6 m in height and is not perpendicular to the slope. The fence was angled 105° to the up-slope.

During a monitored winter (2014-15), the influence of temperature and location was highlighted. Over twelve days, diurnal and nocturnal temperature gradients showed their influence on snowpack pressure in five cells, 2.11. These cells were located on the southern edge, with cell number 1 being on the row closer to the ground.

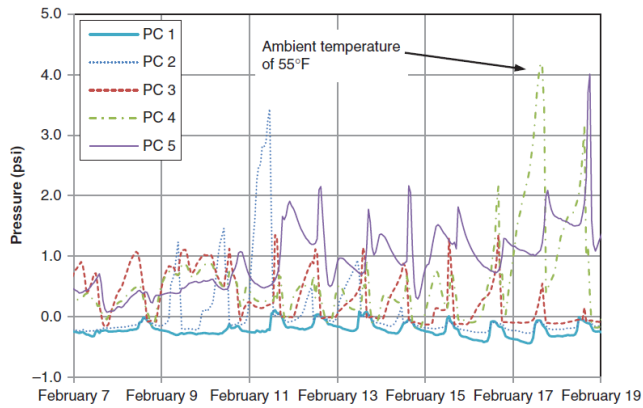


**Figure 2.11:** 12 days snow pressure monitoring over southern edge of support

Mid-February, maximal temperatures of  $12^{\circ}C$  have been recorded which leads to the highest pressure observed on the two top cells. It is observed that maximum pressures are delayed between the different rows. The reason advanced by Hewes et al. (2016) is the bridging and redistribution of internal stress over time and the snowpack. Bridging is a stronger layer resting on a weaker layer. However, this weak layer can still bear a certain load that is difficult to determine.

The pressure cells have been plotted against their row position, see fig. 2.12:

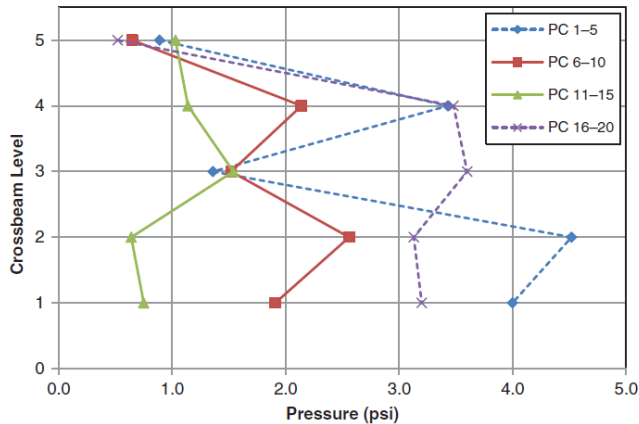


**Figure 2.12:** Evaluation of averaged pressures over the cross beam section

The data point in row 3, PC 16-20, appears to be very far from the trend of the rest of the cell column and is therefore not taken into account in the analysis. As expected, the rows near the edges, PC 1-5 and 16-20 have shown a greater pressure peak with depth.

The end-effect coefficient  $f_R$  can be estimated from the difference between central and side pressures. Hewes et al. (2016) gives an experimental  $f_R = 2.1 \leq F_{Rth} = 4.75$ , this shows how conservative the assumptions made by the Swiss standards are in this case. However, it should also be taken into account that the results are for one winter only and should be treated as such. The end-effect factor of 4.75 may be achieved in-situ in more unfavorable snowpack conditions.

According to the Norwegian results, there should be a maximum pressure on the second row, equivalent to a height of  $0.4 \cdot H$ . The PC columns 1-5 and 6-10 exhibit similar behavior, while the other two columns display a maximum little higher, on the third row. This trend is somewhat analogous to the Norwegian in-situ monitoring data.

## 2.8 Summarizing table

The equations of distributed load, table. 2.3, and back-pressure zone, table. 2.4, are summarized.

Models	Distributed load
<b>Haefeli</b>	$S'_N = \frac{\gamma}{2} \cdot H^2 [(1 - 2 \cdot \tan\beta_{45^\circ} \cdot \cos^3\psi + \frac{1}{3} \sqrt{\frac{2}{\tan\beta_{45^\circ}} \cdot \sin 2\psi \cdot \sqrt{1 + 3n}}]$
<b>Bucher</b>	$S'_N = -\frac{\gamma}{2} \sin\psi \cdot D^2 \cdot \sqrt{\frac{2m}{m-1}}$
<b>Ziegler</b>	$S'_N = -k \cdot \frac{D}{2} \cdot (\cot\psi + \pi)$
<b>McClung</b>	$\bar{\sigma}_x(0) = \bar{\rho}gH \cdot \sin\psi \cdot [(\frac{2}{1-\nu})(\frac{L}{H} + \frac{D^*}{H})] + \bar{\rho}g\frac{H}{2} \cdot (\frac{\nu}{1-\nu})\cos\psi$
<b>Swiss Guidelines</b>	$S'_N = \rho \cdot g \cdot \frac{H^2}{2} \cdot K \cdot N$
<b>Norwegian Guidelines</b>	$\sigma_x = \rho gh \cdot [3.125 \cdot \sqrt{0.25 \cdot \sqrt{\sin\psi} + 0.05 \cdot \sin\psi + 0.28 \cdot \cos\psi}]$

**Table 2.3:** Summary table of slope-parallel pressures models

Models	Back-pressure zone
<b>Haefeli</b>	$y_b = -H \cdot \sqrt{\frac{2}{\tan\beta_{45^\circ}} (1 + 3n)}$
<b>Bucher</b>	$y_b = -\frac{6}{\pi} D \cdot \sqrt{\frac{2m}{m-1}}$
<b>Ziegler</b>	$y_b = \frac{k}{\gamma} \cdot \frac{\cot\psi + 3\pi}{2\sin\psi}$

**Table 2.4:** Summary table of back-pressure models

Looking at the table and with the theoretical work presented above, it can be seen that the only variable as a function of time is the total snow depth, H or D. This variable is present as a single or squared factorization. As we shall see, it does not affect the shape of

the model so much as the amplitude of the pressure variations.

It should be noted that most models (except the Swiss guidelines) provide pressures (kPa) and not linear force (kN/m). To remedy this, a one-meter band perpendicular to the slope is considered in the rest of the study for these models. This will make it possible to compare with the Swiss standard and more importantly the data provided by the snow load device system.

# Chapter 3

## Methods

During the thesis, several methods were implemented to collect data on the creep and pressures of snow on supporting structures. The theory and implementation of these experiments are detailed in this section. Interest is given to the definition of the accuracy and sources of error of the different measurement devices. All fieldwork was carried out in cooperation with Simon Prochaska, a guest master's student at UNIS from the Technical University of Munich. Fieldwork in Svalbard involves several precautions regarding the harsh environment and the presence of local wildlife. The safety measures taken are detailed in the following paragraph. During this thesis, two in-situ sites have been considered. Creeping, snow-pits, and pressure measurements have been carried out at the site called "Shooting range" and studied structures are located on the west slope of Sukkertoppen, see Figure. 3.1:



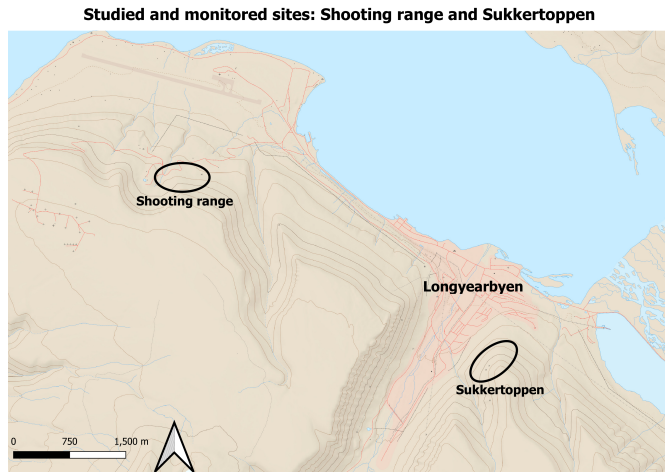


**Figure 3.1:** Location of both monitored sites in Longyearbyen

The monitored site "Shooting Range" is described and detailed in this section, while the characteristics of the site and the structures on the Sukkertoppen slope are elaborated in the Interpretation section, 5.

### **3.1 Hazard linked to fieldwork**

Doing fieldwork in Svalbard requires careful preparation and adaptability. Even though the largest amount of the fieldwork was carried out within the city limits, some hazards had to be taken into account and not neglected. Due to the purpose of the thesis, most of the fieldwork had to be carried out on or near slopes, therefore the danger of avalanches was predominant. Before each fieldwork, the snowpack condition was assessed with the logistics department and whether permission to go out was given or not. All fieldwork was carried out with an avalanche safety kit, a beacon, a probe, and a shovel. Special attention to wind accumulation and other avalanche triggers warnings.

In Svalbard, the fauna is very present and singular, often inoffensive like reindeer but also being able to pose major safety problems: polar bears. Polar bear protection (rifle and flare gun) and guarding have always been part of the fieldwork, requiring at least two people at all times. While the likelihood of encountering a polar bear within the city limits is low, it is not zero and previous lethal cases have proven that a permanent alert is necessary for Svalbard.

At the beginning of the season, the very cold temperature also played a role in the preparation of the fieldwork, as it reached a temperature as low as  $-30^{\circ}\text{C}$  without wind chill.

In these temperatures, static fieldwork requires appropriate clothing, and vigilance when handling a steel device which may require exposing bare hands for example.

## 3.2 Snow Load Device System

Much of the data used in the thesis was collected from an existing snow load device, implemented by Arne Aalberg in 2019. The use of this data is limited and cannot be shared with a third party. This device is located near the site called "Shooting range", just above Longyearbyen airport, see fig. 3.1.

The characteristics of the site are, a slope of 30, with western orientation. It is located in the northern part of the cliff run-out area just above. The soil is composed of sedimentary boulder layers of various sizes and scree types. The set-up consists of a wall placed perpendicular to the slope, mounted with a pressure cell on each corner. The dimensions of the plate are 3 x 1.5m (width x height). Measurement of pressure is the main goal of the device, and some additional parameters are measured such as snow depth, temperature, and humidity, see fig. 3.2:

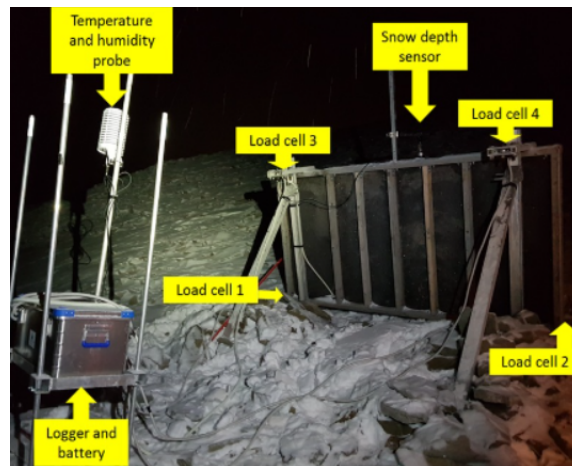


**Figure 3.2:** Snow load testing system implemented in the shooting range site, source: [http://158.39.149.181/Snow\\_wall/index.html](http://158.39.149.181/Snow_wall/index.html)

In Figure. 3.2, the rocky ground cover can be observed, this interface is described as rough. Taking into account this qualification and the negative temperature interface due to the presence of permafrost, this justifies the neglect of the gliding of the snow cover on the ground.

Data have been collected for two spring seasons, 2020 and 2021. Complete data are

processed at the end of the season, and an overview of pressure cells and snow depth is available online for the current spring of 2022. The apparatus system is composed of several elements:

- Force transducer: HBM, S9M/20 kN - Range: - Accuracy: 0.02% relative to full scale value.
- Snow thermistor: Campbell sci, type 107 - Range:  $-35$  to  $+50^{\circ}C$  - Accuracy:  $\pm 2^{\circ}C$
- Snow depth: Campbell sci, Sonic distance sensor, SR50A - Range: 0.5 to 10m - Accuracy: larger value between  $\pm 1$ cm or 0.4% times the distance to the target
- Air temperature and humidity: Vaisala HMP155A - Range temperature:  $-80$  to  $+60^{\circ}C$  - Accuracy:  $\pm 0.226 - 0.0028 \times \text{temperature}$

The detailed excel data is composed of snow force in kilogram for each cell, snow temperature at depths of 0, 35, 70, 105, and 140cm, air temperature and humidity at 2m, and snow depth. Measurements of each of these parameters are recorded every hour.

### 3.3 Snow creep measurement

In addition to the load data, a set-up was made to estimate the snow creep on the test site. In-situ creep data are not so common in the snow research area. There is no standard method of measurement, which is mainly due to significant disparities in snow conditions from day to day and from location to location. In the past, a few papers have addressed the problem with varying degrees of success. Caselli (2004) provides a comparison of 3 methods he used to measure the creeping process in the San Juan Mountains, Colorado. The set-up chosen for this thesis was inspired by his work, accounting for the Svalbardian snow pack specifications. Caselli's paper is presented briefly in the next section.

#### 3.3.1 Caselli's comparison of set-ups

Caselli (2004) implements three methods using sawdust, measuring tape, and wooden stakes, during the same winter. The principle of the first experiment is replacing snow with a material that will deform similarly. Saw dust has been chosen and used, by McClung already, and presents an acceptable similarity to snow, especially regarding porosity. Naturally, not all snow is identical and Arctic snow is likely to have properties that require packed sawdust or other material. The downside of the method is that it is only possible to collect the deformation once. Therefore, it is not possible to monitor deformation with

time, over a winter.

In 1994, Walker (1994) has first used a measuring tape to observe strain. Measuring tapes are fixed to a waterproof box and attached to a metal plate dig into the snowpack. Caselli has repeated the experiment with some adjustments, this method allows the monitoring of deformation in function of time, which is a strong asset. Caselli (2004) reported some problems with the burial of the device by newly fallen snow and the simultaneous recording of creep and settlement. On my end, an installation of this method has been attempted at the site. However, it showed difficulties in achieving a fixed point, and the plates were damaged by polar foxes.

The last experiment presented in the paper is using wooden stakes. The poles are buried at different depths, and a line materialized by two fixed points allows the researcher to survey the movement of the stakes. This method has been the one chosen to be implemented in this thesis. Some adaptations have been made in relation to site constraints.

### **3.3.2 Preparation and set-up**

Wooden stakes have been furnished by a local construction company, LNS Spitsbergen, and two different areas of poles have been used: 2 x 5cm and 1.5 x 3.8cm. To monitor creep at different depths of the snow-pack, poles have been cut down to a length of 230cm on average. The set-up of the stakes has been a bit more challenging than expected, partially due to the high degree of stiffness of the snowpack. We have managed to drill down to the ground the smaller area poles. However, it was not possible for the large poles, therefore they have been only inserted until 80cm.

In total 6 stakes were put in place at different depths in a line, perpendicular to the slope and at each side of the snow load device, 3.3 and the implementation location is visible on figure 3.5

The only fixed point available is the snow load system, therefore stakes have been aligned with respect to it. After some weeks of implementation, the stakes have undergone large tilting and have been covered by snowfall and wind drift.



(a) Installation set-up - Creep measurement



(b) Angle measurement using Nikon Forestry Pro along the wooden poles

**Figure 3.3:** Creep measurement set-up

### 3.3.3 Monitoring

Assumptions and hypotheses behind the angle measurement are the following:

- Wooden poles are hammered perpendicular to the slope
- Stakes inserted to the bottom are assumed to be fixed on their lower part. Therefore, poles can only move by tilting.
- In this case, creeping is assumed to have a triangular distribution over the pole and creep is expressed as a resultant displacement, placed at  $2/3$  of the stake
- Sinking of the poles inserted mid-layer is neglected

In view of the snowpack's high stiffness, the validity of these assumptions is accepted, simplifying further calculations and analysis. Monitoring of the wooden posts has taken place weekly since 22/02/2022, the date of implementation. Two methods were employed to record creep, using angle variation and down-slope displacement of the stakes. Angle variation is measured using a laser telemeter, Nikon Forestry Pro, see fig. 3.3b. Its accuracy is down to  $0.1^\circ$ . The procedure is simple. The device is placed along the pole, close to the ground to avoid movement of the stake. Then, five measures are averaged for each pole, in order to reduce operating errors. This method assumes that the poles will tilt under creeping of the snowpack.

Direct measurement of the displacement of the stakes, in the direction of the slope, is made. Using the snow load device as a fixed point and a measuring tape placed perpendicular to the slope, the advancement of the sticks is monitored weekly. This method allows for direct measurement but leads to greater uncertainties due to the difficulty in repeatability. Therefore, the measurements will not be presented in the results and will only be used as a progress check with no measurement purpose.

### **3.3.4 Errors sources**

Unfortunately, this experiment also brings out also approximations. It is important to estimate these errors in order to assess the confidence that can be placed in the results. Between the device error and the user error, the total margin of error was determined to be  $\pm 0.5^\circ$ , which leads to a margin of error of  $\pm 0.1\text{cm}$  in creeping results.

## **3.4 Snow pits**

As stated in the literature review, snow density and temperature are the most important parameters influencing snow pressure. The assessment of snow density is only done on an ad hoc basis, through snow pits, and not as a function of time. Temperature is monitored all winter long, thanks to thermistors installed in the Snow load system, 3.2. However, the temperature was still recorded for each depth where a density sample was collected. During this thesis, one snow pit was dug per week in order to follow the evolution of the snow density, establish a reasonable density function for the Svalbard snow, and also to compare it with the evolution of the snow pressure.

### **3.4.1 Description of the different tests**

Digging a snow pit is the best method to characterize the properties of snow layers. The snow is studied directly with little reworking. However, the procedure is relatively time-consuming and is only repeated weekly, while the pressure data is updated hourly. From the snow-pit, several data are gathered, density, layering, temperature, slope angle, and hardness. Other parameters can be collected but were not relevant for the thesis, such as grain size, shear stresses, etc. The material used is shown in the figure. 3.4c: avalanche probe, thermometer, shovel, scale, and cylindrical snow sampler in aluminum.



(a) Digging of snow pit - 23th February 2022



(b) Snow core for density measurement - 20th April 2022



(c) Snow pit equipment - 20th April 2022

**Figure 3.4:** In-situ testing: snow-pits

The measurements are done in several steps:  
Firstly, the layers are determined according to differences in hardness and grain size. The hardness is classified by symbol, corresponding to the penetration of various items: a fist (Fist), 1 to 4 fingers (1-4F), pen (P), or knife (K). Once the snowpack has been separated into layers, the density of each layer is estimated. A cylindrical sampler of known volume and mass is used. Two snow cores are taken from each layer. The samples are weighed in situ. Finally, the temperature of the snow is recorded for each depth selected during sampling.

### 3.4.2 Errors sources

Sources of error arise in particular from the density measurement. Due to the granular nature of the snow, the filling of the cylinder may not be accurate. Therefore, an estimate of the margin of error should be made. The scale, Sartorius AY4000, has a  $\pm 0.1\text{g}$  accuracy and will not have a determining influence on the error assessment. On the other hand, the process of coring and positioning on the scale results in a larger loss of accuracy. After several weeks of snow-pits, it has been determined that this error can be estimated at  $\pm 5\text{g}$ . The thermometer TH310 by Milwaukee is accurate to half a Celsius degree ( $\pm 0.5^\circ\text{C}$ ) according to the seller.

## 3.5 Implementation in-situ testing

During the fieldwork, GPS coordinates of the snow pits and creeping stakes were recorded. The location of each measurement was depicted in the figure. 3.5:

### Shooting range - Test Site

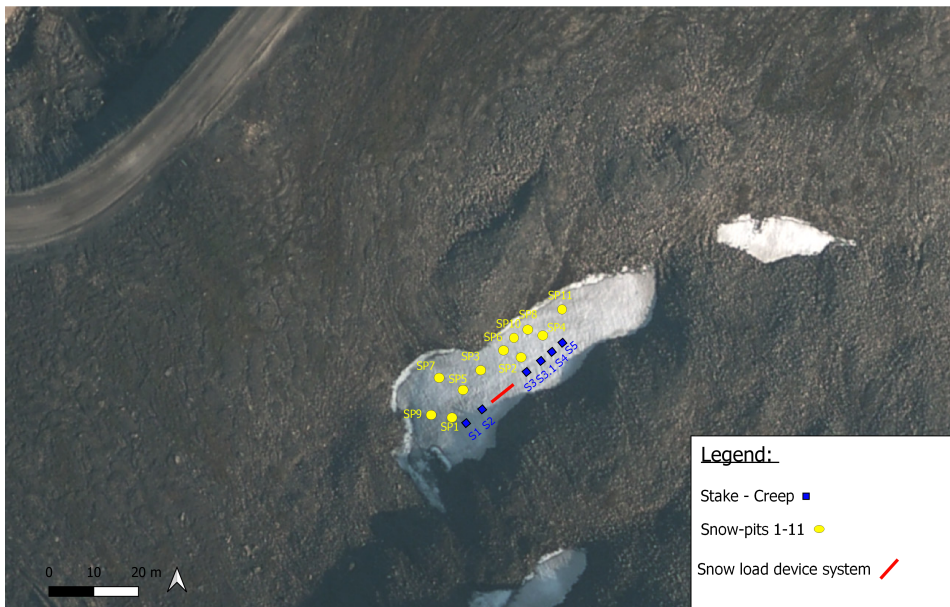


**Figure 3.5:** Position of snow-pits and creeping stakes near the snow load device



## Results: in-situ data

This section compiles and presents the overall results, from the fieldwork campaign and snow load device. Descriptions of the data and correlations are sketched here, but discussions and interpretations of the models are left for the next chapter, 5. The data was collected and assembled in Excel. The analysis has been conducted on Jupyter in Python language. All results have a temporal indication, to highlight the influence of the season period on the evolution of the loads. Snow-pit density and temperature, as well as creep data, were collected in spring 2022.

While the complete collection of snow load device data is done in summer when all the snow is gone. Therefore, the available complete data from the snow load device corresponds to the two previous springs, 2020 and 2021, summarised in table 4.1. A partial set of load data is available online for spring 2022 and has been plotted further on. However, no snow depth data is available yet for 2022, which prevents any model comparison.

<b>Data collected</b>	<b>Time period</b>
load cells	Spring 2020/21
Snow depth	Spring 2020/21
Thermistors	Spring 2020
Snow-pits: Density, temperature	Spring 2022
Creep	Spring 2022
Incomplete Snow load data	Spring 2022
Main warm event (+5°C)	14 to 18 of March 2022

**Table 4.1:** Data collection season

Particular attention has been paid to the spring of 2020, as it has the most detailed data set. It includes snow temperature at different depths, which leads to the calculation of temperature gradients.

## 4.1 Snow pits

The snow-pit data is divided between density and temperature readings within the pit. A total of 11 pits were dug during the thesis, starting on 23 February 2022, and ending on 24 May. The aim was to have a weekly survey of these two properties. An additional parameter of hardness has been studied but will not be presented here due to low correlation with load and high variability within the snowpack and season. Two weeks were missed due to the Easter holidays and unexpectedly hot weather in mid-March, which resulted in positive temperatures and heavy rainfall, making the site inaccessible. The implications of this last event will be discussed in more detail in the 4.4 section.

Both data were associated with a depth measurement, in-situ. The measurement error was estimated to be  $\pm 1$  cm relative to the graduation on the probe. Throughout the season, the total depth reached in the snow pits varied from 1m to 2.7m. The location of the snow-pits has been monitored using a GPS and is presented in 3.5. For each data point, the uncertainty has been calculated in the methods section for the directly measured parameters. The error bars are shown on the graphs, the depth scale is too large to appreciate the error bar on the y axis.

### 4.1.1 Density

The dense stratification of the snowpack has generated changing densities. The presence of narrow well-defined ice lenses resulted in a more difficult digging procedure and sampling. As mentioned in 3.4.1, sampling is done with an aluminum cylinder. Driving this sampler into the layer is made increasingly difficult with increasing density, and impossible in ice. The decision was made not to include these ice lens data points in the graph due to the loss of clarity caused by very high-density points. Densities are expressed in  $\frac{kg}{m^3}$ . The margin of error of direct weight measurement was set to  $\pm 5g$  when defining the methods. Therefore, the density error corresponds to, assuming that the volume of the sampler is a known constant:

$$\frac{Estimated\ error\ [g]}{Volume\ sampler\ [cm^3]} = \frac{5}{508.95} = 9.82 \approx 10 \quad [kg/m^3] \quad (4.1)$$

As a result, the snow densities for all excavated pits are presented in Fig.4.1. The error on the density is quite remarkable, while the error bar on the depth is merged with the size of the data point.

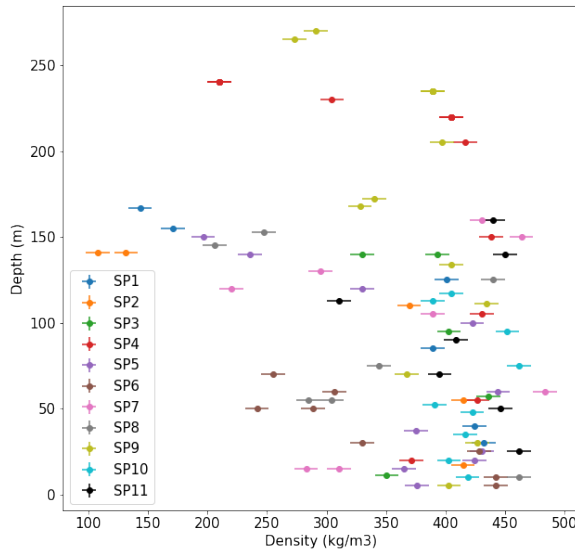


**Figure 4.1:** Snow density with error bars - Spring 2022

Looking at the distribution of density as a function of depth and season, it appears that density is more sensitive to snow depth than to the time of year. The density is very scattered over depth and the only clearly visible trend is the location of lower density on the surface layers. Secondly, depth does not seem to systematically increase density. Low-density layers are visibly buried around 50cm depth for SP6 and 8. The warm period that occurred between SP4 and SP5 also did not clearly influence the density.

### 4.1.2 Temperature

Temperature data from the snow pits were taken for cross-checking purposes. The readings were aimed to be taken at the same depth as the coring. Uncertainties bars for both axes,  $\pm 0.5^{\circ}C$  on x and  $\pm 1cm$  on y, are merged with the size of the data point. Therefore, they are not visible in the figure. 4.2:

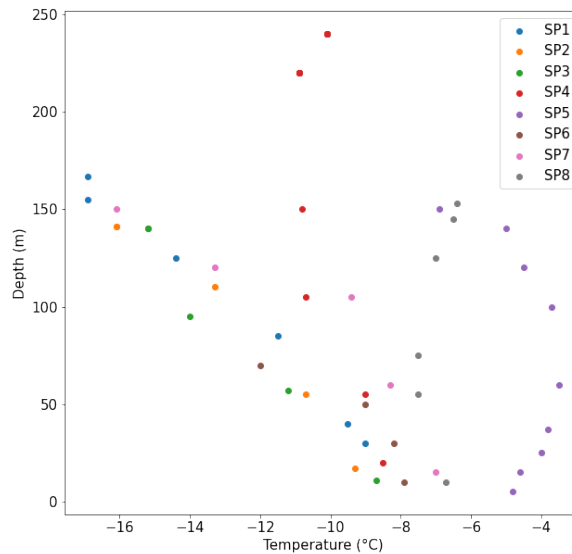


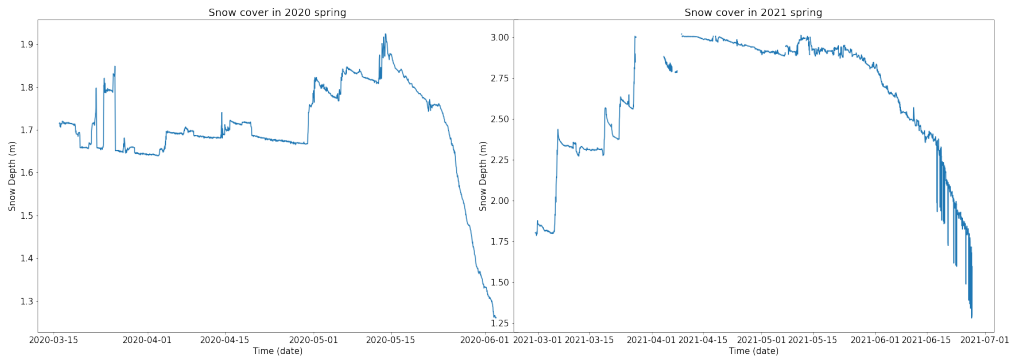
**Figure 4.2:** Temperature measured in the pits - Spring 2022

The layer temperatures in the snowpack are quite scattered. However, the trend shows a cold pack at the beginning of the season, with overall warming until SP5. SP5 corresponds to the pits dug just after the March warming week. Snow-pack temperatures were abnormally high. Just after this warming period, the air temperature dropped sharply to  $-15/20^{\circ}\text{C}$ . The first layers of the snowpack were very cold. The cause was that the increased high water content of the snowpack froze, generating this sharp drop in temperature, most visible at the top of the snowpack, SP6 & 7. Longyearbyen ground is composed of an active layer, i.e seasonal permafrost, and overlying permafrost. The presence of this active layer plays a role in keeping the bottom boundary at a relatively low temperature, between  $-6$  to  $-10^{\circ}\text{C}$ . These low temperatures, near the ground, contribute to keeping the temperature gradient low. A problem with the thermometer prevented the snow temperature from being recorded for the last pit dug.

## 4.2 Snow load device system

### 4.2.1 Snow thickness

For both springs 2020 and 2021, snow depths are available and have been plotted. Spring 2021 had exceptionally high precipitation, even leading to the depth sensor reaching its maximum reading. The sensor is installed on a 3m mast. We can observe a period, in early April, see figure. 4.3b, where the data is missing. The reason for this is that the sensor was buried in the snow. The extent of the snow cover is also much greater in 2021, over about 1 month. A depth of 1.30m was reached at the beginning of July, whereas in 2020 the snow had melted to this depth by the beginning of June, see figure. 4.3a. Snow depth is one of the input parameters used in the models. Therefore, when calculating the equations for the different models, the missing data were replaced by a conservative 3m of snow cover in the Excel sheets.



(a) Snow depth throughout 2020 spring

(b) Snow depth throughout 2021 spring

**Figure 4.3:** Snow depth data extracted from the Sonic distance sensor

The snow cover at the beginning of March is equivalent for both springs, at around 1.7m. However, in 2020, precipitation remains low so the variability of the depth is also low. A maximum snow depth of 1.9m is reached in mid-May. In 2021, as with load, a gradual increase in snow depth is observable, reaching 3m of snow depth and then remaining relatively constant until June, 4.3b.

## 4.2.2 Snow load

All the models, presented in the literature review, have defined the snow load, or pressure, in the snowpack as distributed, constant over depth. However, the device data is provided as four-point loads in kilograms. As stated in the methods section, the cells are located on each corner of the plate, meaning the load recorded is affected by the end-effect. The first step is to convert to a force in kilo Newton:

Snow force [kN] = 0.00980665 · Snow load [kg]

The aim is to have a distributed load over the height of the plate,  $\frac{kN}{m}$ , to be analyzed along with the models. The two forces of the lower and upper cells are averaged in pairs. Thus, only two forces are defined on the plate, one on the lower part and one on the upper part. The plot of these two forces is available in appendix 6.2 and shows an upper load more than double the lower load. This phenomenon will be correlated with the creep data to suggest an interpretation. To compare these data to the models, the resultant,  $F_{Resultant}$ , is calculated as follows:

$$F_{Resultant} = Force_{Bottom} + Force_{Top} \quad [kN] \quad (4.2)$$

$F_{Resultant}$  is assumed to be evenly distributed over the wall, see figure. 4.4. This assumption does not represent the reality of the snow load distribution over the depth. It is simplistic but also made by the design models, which makes it necessary for comparative purposes. A more realistic load distribution has been made in Appendix n° 6.4. With this goal of uniform load, the resultant,  $F_{Resultant}$ , is divided by the plate height. Therefore, the load is expressed in uniform over snow depth.

$$Uniform \ load = \frac{F_{Resultant}}{Height} \quad [kN/m] \quad (4.3)$$

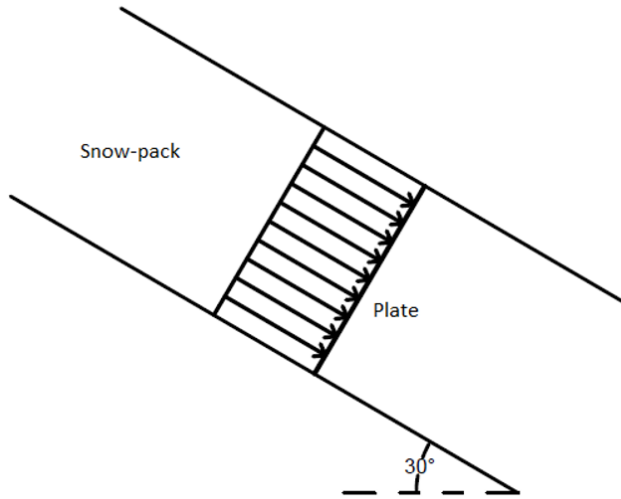
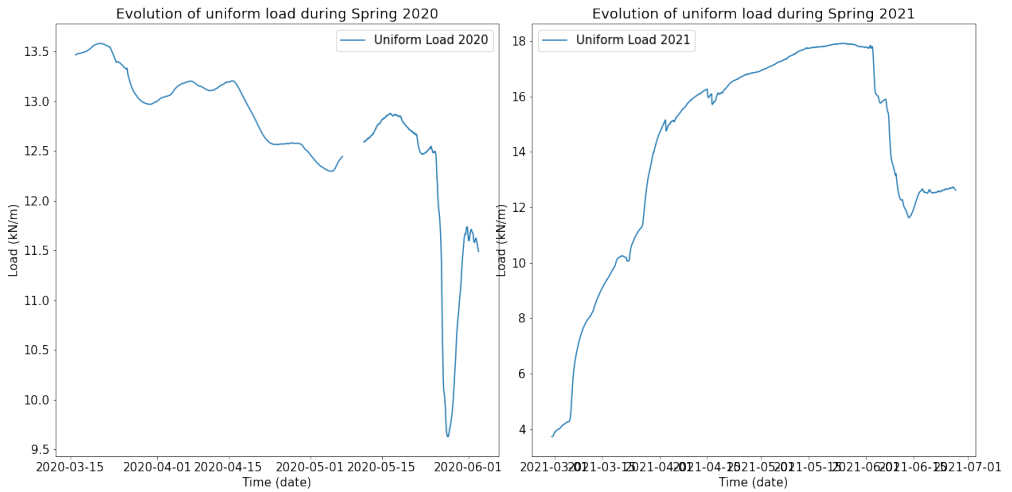


Figure 4.4: Uniform load scheme

Uniform load is expressed in function of the time for both 2020 and 2021 spring, in figure. 4.5:



(a) Evolution of uniform load during Spring 2020

(b) Evolution of uniform load during Spring 2021

Figure 4.5: Uniform load for both Springs

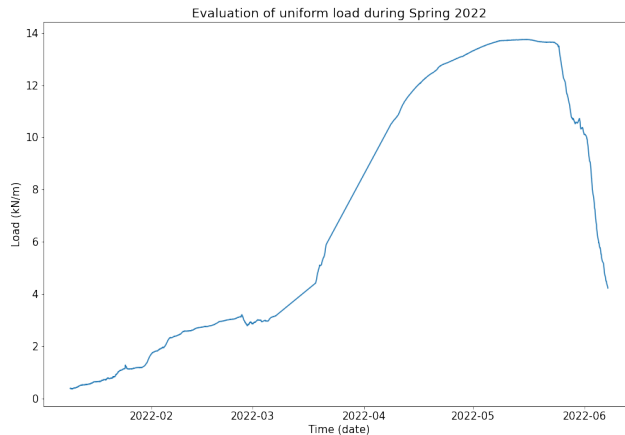


**Figure 4.6:** Evolution of uniform load during Spring 2022

The evolution of snow load throughout the season is fairly distinct between 2020 and 2021. From March on-wards, in 2020, the snowpack load is already well established, and only declines from then on. Whereas, the load build-up is visible in 2021, and will reach its full extent at the end of May, and then will experience a sharp drop. The maximum load reached in 2021 is 33% higher than in 2020. One of the directly measured factors that can be correlated to this load difference, is the snow depth, described in 4.2.1. In 2022, the snow load increased significantly at the end of March. Unfortunately, the monitored snow depth could not be collected. However, according to my experience in the field, the maximum snow depth reached between 2 and 2.30 m, thus lying between 2020 (lower) and 2021 (higher). This corresponds to the maximum load amplitude, which also lies between the two values in the data sets.

### 4.2.3 Snow temperature

As previously emphasize, snow, and ambient temperature to some extent, play a major role in snow loads. Thermistors have gathered data at 5 different depths during Spring 2020, 0 cm, 35cm, 75cm, 105cm, and 140cm and an extra sensor was implemented for air temperature readings. These data are only available for spring 2020.



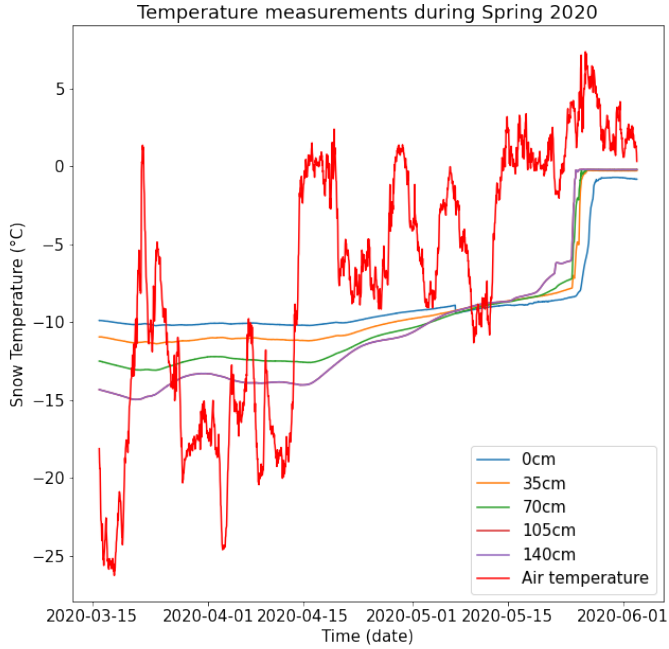


**Figure 4.7:** Snow & air temperature measurements during Spring 2020

From the figure 4.7, 3 time periods can be identified for the two types of temperature, and summarized in tab. 4.2:

<b>Time period</b>	<b>Snow temperature</b>	<b>Air temperature</b>
<b>1</b>	mid-March / start of May	mid-March / mid-April
<b>2</b>	start of May / end of May	mid-April / mid-May
<b>3</b>	end of May / June	mid-May / June

**Table 4.2:** Temperature period from data collection

When comparing time periods of air temperature and snow, in tab. 4.2, it shows that snow reacts with a delay of 2 to 3 weeks to changes in air temperature.

By observing the snow temperature, figure. 4.7, the isolating effect of the snow is highlighted. Indeed, in mid-winter, the air temperature is much colder than the snow temperature. Therefore, the thermistors near the surface record lower temperatures than those near the ground. Over the first period of time, the temperature gradient is about  $4^{\circ}C$

within the snowpack. The complete evolution of the temperature gradient is plotted in section 4.8. But during the season, the temperature gradient decreases strongly until it is even reversed at the end of May. This is the effect of the sun and the air temperature on the snow. In March, it contributes to the cooling of the snowpack, but from May onwards, the sun's share in the warming of the snowpack increases more and more, leading the top layer of the snowpack to exhibit the highest temperatures. Older snow tends to have a lower albedo, due to the metamorphism process and the presence of impurities, B and Haider (2016). Lower albedo leads to more heat absorption by the snowpack. On the other hand, the presence of permafrost contributes also great at keeping the bottom thermistor colder than the rest of the snowpack in May/June. From the thermistors placed at 0cm at 140cm, the temperature gradient is calculated,

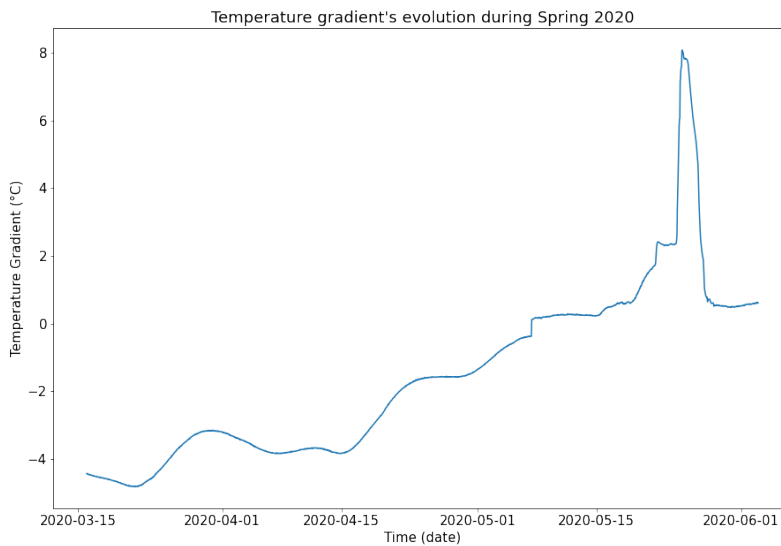


**Figure 4.8:** Temperature gradient calculated for 140cm snowpack - Spring 2020

The evolution of the temperature gradient is interesting to analyze. Until mid-May, the expected behavior is seen, negative gradient, meaning the top thermistor record colder temperature than the ground thermistor. The maximum gradient was reached in early March, corresponding to an absolute value of  $4^{\circ}\text{C}/1.40\text{m}$ . This represents a gradient of  $2.86^{\circ}\text{C}/\text{m}$ , which is quite far from the set limit of  $10^{\circ}\text{C}/\text{m}$ . However, the temperature gradient reverses at the end of the season. This is due to the warming of the air temperature and the melting of the snow cover, which causes the 140 cm thermistors to move closer

to the surface. It is also due to the fact that the permafrost keeps the ground at a low temperature for longer. At this point, the gradient reaches a value of  $5.7^{\circ}\text{C}/\text{m}$ , which is still far from being considered high ( $10^{\circ}\text{C}/\text{m}$  limit). Within a few days, equilibrium is restored and the gradient becomes zero.

### 4.3 Snow creep

As mentioned in the methods chapter, the creep data has been gathered throughout the 2022 season in the form of tilt angle differences. In order to use the data for creep analysis, the tilt differences have to be converted into displacement. In order to convert these data, an assumption about glide must be made. In our case, the glide is assumed to be zero for the stakes, frozen and coarse soil, i.e. seasonal active layer of the permafrost, have induced this hypothesis. This assumption is somewhat reductive, but it is confirmed fairly well by cross-checking the downhill movement of the wooden poles with the tape measure, as explained in 3.3.3.

An important discovery changed the interpretation of these results. At the beginning of June, during the last angle survey and end of the fieldwork campaign, it was found that all the stakes were broken in two, at a similar average height of 1.2 m from the ground. This breakage was not certain until now but was strongly suspected given the high inclination of the poles coupled with their low down-slope movement. The part of the stakes that did not break, kept an angle of inclination closer to the one at which it had been implemented. This observation supports the hypothesis of no glide of the snow-pack. Therefore, two different creeping velocities have been calculated. One represents the bottom part of the snow cover, up to 1.20m, and another one displays the upper part, from 1.20 to 2.20m high. These heights were determined by reading the scale previously marked on the poles. Pictures of the broken poles taken in June 2022 are available in Appendix. 6.6.

Thus using the geometry of the experiment and knowing angles, it is possible to calculate the average creep of the pack, as described in Appendix n°6.5. As shown in the illustration, 4.9, creep is represented as depth-dependent.

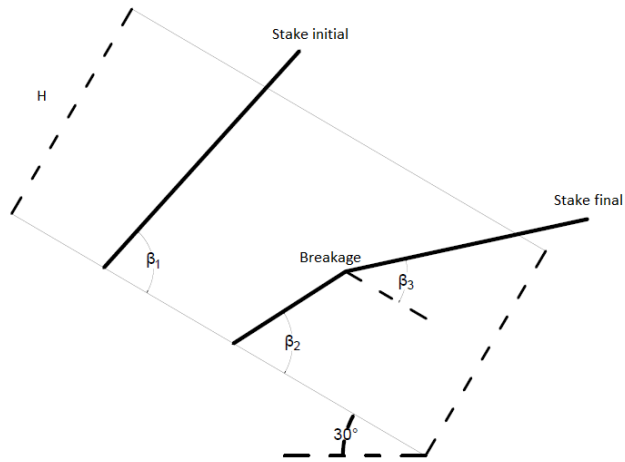
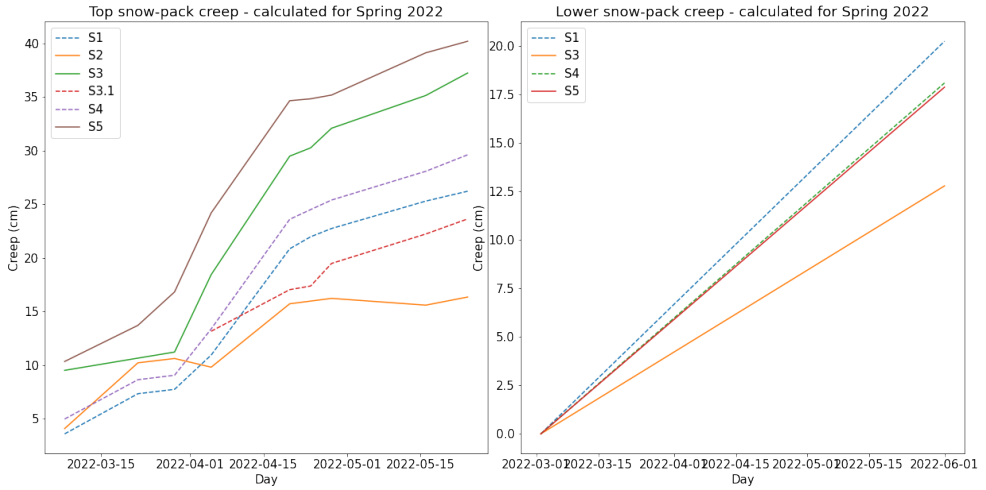


**Figure 4.9:** Creep calculation and movement

The evolution of the cumulative creep is interesting to plot, see figure. 4.10, because it gives information about the speed at which the stakes inclined, over the whole duration of the experiment. Whereas, the evolution of velocities, between each reading, highlights the period of high and low creeping, 4.11.



(a) Accumulated creeping at the bottom of the pack      (b) Accumulated creeping at the top of the pack

**Figure 4.10:** Results - In-situ creep measurement

The three stakes inserted at a depth of 80 cm are shown as dotted lines in the figure. 4.10. In figure. 4.10b, stake number 2 is not shown because the stake did not break and therefore the angle is the same all along. The angle was not recorded because it was not representative after most of the pack had melted. Pole number 3.1 is also not shown because it fell before we could measure the angle. It can be seen from the figure. 4.10a, that the stakes are increasingly inclined because high creeping is equivalent to high tilting. It is possible to hypothesize about the period of breakage of the poles. The strong changes in slope, that takes place at the beginning of April, could match with the breaking in two of the stakes. Knowing that this corresponds to a period of two weeks after the mid-March warming period, these two events are probably related. Indeed, this period disrupted the constitution of the snow-pack, making it very wet, then stratified with layers of ice created by the sudden cooling at the end of March. The three stakes, inserted in the middle of the snowpack (dotted line figure 4.10a), show a very similar evolution of inclination with time, indicating that the aim to measure this snow-pack height worked relatively well. Then, we observe a variability of inclination for the poles inserted to the bottom of the snowpack. Stake n°2 (S2) had little tilt over the season, recording a decrease in angle of 25%. Conversely, stake n°5 (S5) dropped 60% in angle. The reasons given for these dissimilarities could be a difference in the layers monitored, leading to different creep rates. Snow-pack properties are not uniform over an area and different load and creep rate

distribution have led to a pole being broken or only bent. Stakes S5 and S3 follow the same trend, with a different amplitude. This suggests that these poles measured the same layer movement.

The graph. 4.11, allows to distinguish more directly the different periods of creep speed. There is no overall trend for the season as a whole. The only period where the majority of poles are in agreement is the period of strong creep in April and the subsequent sharp slowdown, see S1, 3, 4, and 5.

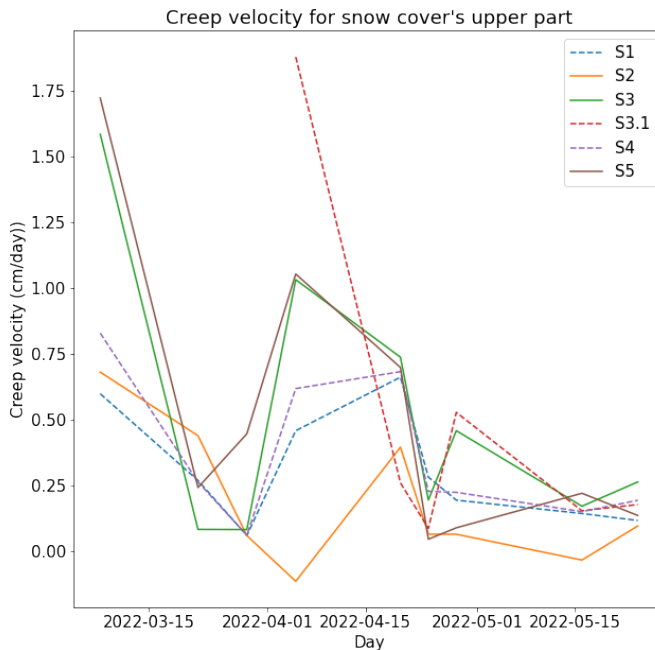


**Figure 4.11:** Creep velocities parallel to slope for the upper part

## 4.4 Correlation Study

In this section, the possible correlations between the factors presented above are examined. Firstly, the link between air temperature, creep and the potential impact on the load recorded for the spring of 2021 will be investigated. The air temperature is taken at the airport weather station, the closest to our site. The study period, provides the following data, see figure. 4.12. Data have been retrieved from the weather website, yr.no.

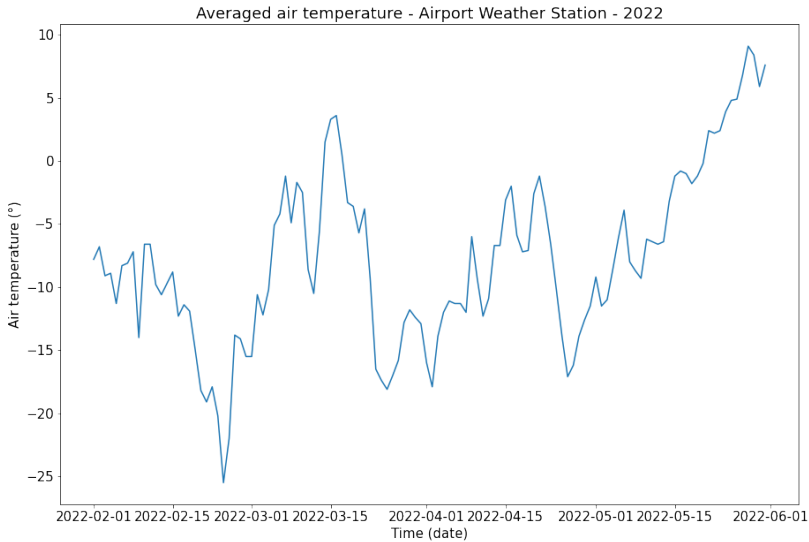


**Figure 4.12:** Airport Weather Station - Average air temperature - Spring 2022

The creep and creep speed values, shown in Fig. 4.10 and 4.11, indicate that the period of strong creep is observed about two weeks after the mid-March warming period, 4.12. It is tempting to link the two phenomena, but without hourly snow temperature and creep data it is not possible to confirm or deny this. However, the creep and load data also show similar trends which could be linked to this episode. Indeed, in the figure 4.6, it can be seen that the very rapid increase in load coincides with a high creep rate in figure 4.11. Points in favor of this explanation are that precipitation remained low over the whole period and the wind was constant for the season, Appendix 6.8, which reduces the scope for other possible reasons. However, a significant snowdrift effect was observed from one week to the next, also contributing to the increase in pressure within the pack. A direct relationship can be drawn between the temperature of the second part of May, fig.4.12, and the large load loss seen on figure 4.6. The end of May was the warmest in the history of weather data at Longyearbyen, chapter 1. This has a direct effect on the melting of the snowpack and decrease in pressure.

Snow pits' temperatures and densities data are too scattered to allow a correlation with the evolution of the load over the same period. The density data for 20 March to 20 April, i.e. SP5 to 8, do not exhibit any trend that can be linked to the sudden increase in load.

For spring 2020, the temperature gradient, 4.8 and load data, 4.5a, have a very similar shape. A threshold value at the beginning of March, then a gradual reduction, and a significant peak at the end of May 2020. It is interesting to note that the inversion of the temperature gradient has a very reducing effect on the load. It is even more striking to note that the load value increases again to a more expected value for the season, which also corresponds to the temperature gradient returning to around 0°C. The importance of the temperature gradient on the pressures inside the snowpack, as outlined in the literature, seems to be consistent with these observations.

As stated in section 4.2.2 and found the Appendix 6.2, a significant difference in linear load between the bottom and top of the plate was observed. In general, an increase in density with depth is observed, which should contribute to the increase of pressures. However, as introduced by McClung and Schaerer (2006), the pressures and loads are produced at 90% by creep. The set-up implemented at the side of the site has shown a significant difference in the amount of creep within the snowpack, comparison between figures 4.10a & 4.10b. The breaking of the posts around the mid-pack revealed two creep rates, for the upper and lower part of the snowpack. That of the upper part is much higher. These observations may indicate the reason for such a large difference in loads between the upper and lower load cells, being a greater creep of the upper part of the snowpack.



## Models interpretation

As mentioned in the previous introduction, two sites are considered during the analysis. The model's equations are based on site characteristics and other parameters that are not necessarily site-specific. The definition of these parameters is of paramount importance for the proper functioning of the models and their comparison with the data, as well as for the sizing of the structures. The determination of these parameters will be detailed here. These characteristics can be listed as follows:

- Density,  $\gamma$  or  $\rho$  [ $\frac{kg}{m^3}$ ]
- Slope angle,  $\psi$  or  $\alpha$  [ $^\circ$ ]
- Snow thickness, D [m]
- Snow height, H [m]
- Structure height,  $H_{structure}$  [m]
- Glide factor, N [-]
- Creep factor, K [-]

And there are also parameters that do not depend on the site, such as :

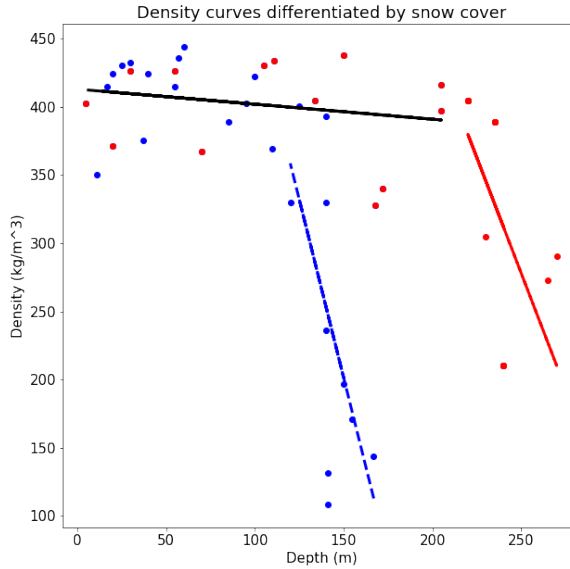
- gravitational acceleration, g [ $\frac{m}{s^2}$ ]
- Poisson ratio,  $\nu$  [-]
- Creep angle,  $\beta$  [ $^\circ$ ]

The characteristics have been defined through field surveys, experiments and literature, especially during the implementation of the load force recording system.

## **5.1 Density from Snow-pits**

The first property to be evaluated is the density of the snowpack because it serves as an input parameter and is variable during the season. The definition of the Svalbardian snowpack density is critical, in the sense that it has a great influence on the formulation of the models and is one of the main means to characterize the local specificities of the snowpack. However, unlike snow depth, its readings are not monitored in a way that allows them to be used directly in the models. In the first part of the thesis, 1, it was argued that the characteristics of the Arctic snowpack differ from those of the Alpine snowpack and therefore require a separate analysis of the loads exerted by the snowpack. These loads are mainly controlled by the temperature and density of the snowpack. After the presentation of the density values recorded during snow-pits, an attempt to differentiate two density values was made. No clear trend of increasing or decreasing density over the season was observed. The differentiation of two density curves is done by the total snow depth of the pack.

From the results section, 4.1.1, a site definition of the density must be made. By splitting the density data into two maximum snow-pit depths data sets, a separate density analysis could be done. The densities corresponding to the two max depths were plotted in Figure. 5.1. In this representation, the axis has been swapped, density is found on the ordinate axis, and the depth on the abscissa,



*[Blue data: Snowpack maximal height] ≤ 1.65m ≤ [Red data: Snowpack maximal height]*

**Figure 5.1:** Snow densities curves, define by snow thickness

A major density trend is derived from the average density over the selected high-density interval, the black line in the figure. 5.1. A distinction is made for two distinct snow-pit depths,  $\pm 1.65\text{m}$  (blue) and  $\pm 2.85\text{m}$  (red). These heights correspond, as far as possible, to the snow depths reached in 2020 and 2021 respectively, as presented in the load data, 4.2.1. In order to input this distinction in density behavior in the models. An idea of implementation of averaged density over the plate height is made. Plate height being 1.5m, an average density (depth  $\leq 1.65\text{m}$ ) is calculated for both data-set.

Data set	Density [kg/m <sup>3</sup> ]
Shallow snow-pack (blue)	350
Thick snow-pack (red)	400
Recommended design density Larsen (2000)	500

**Table 5.1:** Density differentiation based on snow-pack depth

The recommendation on design snow density determined by Larsen (2000), was pre-

sented in the table. 5.1, for comparison. When calculating the loads for the Sukkertoppen site, the design parameters are preferred.

## 5.2 Site Characteristics

Among the two sites considered for interpretation of the models, several parameters are common values for both, as defined in 5.2. The well-known gravitational acceleration,  $g$ , is set to  $9.81 \frac{m}{s^2}$ . Poisson's ratio and creep angle require a more detailed definition to fit the Svalbard environment.

### 5.2.1 Common parameters

#### Poisson's ratio

As detailed in the section 2.2.4, Teufelsbauer is the only one to have addressed the definition of Poisson's ratio as a function of snowpack temperature and density,  $\nu(\rho, T)$ . From the equation 2.36, Poisson coefficient was plotted against the 2020 snow data, temperature, and density, see figure. 5.2. The results show a weak response to temperature changes. While the density was kept constant, due to the snow depth being less than 1.65 m and following the previously stated criteria for snow density.

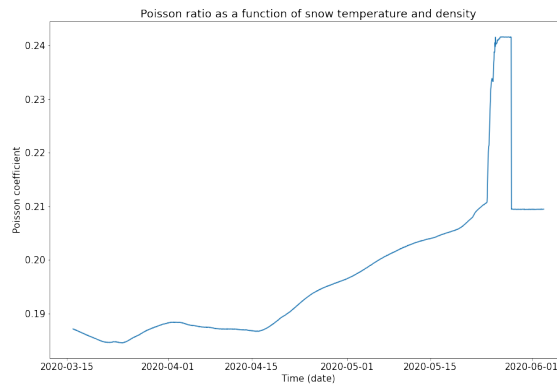


**Figure 5.2:** Poisson's ratio,  $\nu$ , in function of snow temperature and density in 2020's spring

From Teufelsbauer (2011)'s envelope, 2.6, and the density range determined in the previous table. 5.1, an estimate of expected Poisson ratio ratio can be determined.

$$350 \leq \rho \leq 450[\text{kg}/\text{m}^3] \rightarrow 0.1 \leq \nu \leq 0.32[-] \quad (5.1)$$

Lastly, a reminder of Larsen (2000) formulation, which takes into account snow-pack maritime environment particularity. He sets  $\nu = 0.36$ . During the model's interpretation, it has been chosen to use Larsen (2000) Poisson's ratio. Because he accounted for mainland Norway's maritime weather, which is comparable to a certain extent to the one of Svalbard. The Poisson's ratio found by Teufelsbauer's definition also seems too low for the dense snow of Svalbard.

### Creep angle

Creep angle is only used as such by Haefeli (1948). He used a fixed value of creep angle,  $\beta_{45^\circ}$ . Therefore, the tangent of  $\beta$  is not a function and remain constant. Haefeli (1948) set  $\tan(\beta_{45^\circ}) = 0.285$ .

As indicated in the framework section, McClung (1982) also defined the creep angle in terms of Poisson's ratio, equation. 2.29. However,  $\nu$  is preferred in the writing of the pressure equation, 2.32.

### Summarizing table

The values of the common parameters, selected for interpretation, are summarised in the following table: 5.2:

Parameter	Symbol	Unit	Value
Gravitational acceleration	g	kg/m <sup>3</sup>	9.81
Creep angle tangent [Haefeli (1948)]	$\tan(\beta_{45^\circ})$	°	0.285
Poisson ratio	$\nu$	-	0.36

**Table 5.2:** Invariant parameters for both sites

## 5.2.2 Site: Snow load device

The study site near the shooting range, used to collect the data, was presented in detail in the methods section, 3. The site, located on a west-facing 30° slope at an elevation of 253 m, requires the assignment of certain site-specific parameters.

From Swiss Guidelines (2007), creep and glide factors, K and N, are determined. Table 2.2 calculate K, knowing snowpack density and slope angle. Therefore, K is set to 0.80. The slip glide is assumed to be zero, so N is set to 1 so as not to influence the load equation. The end effect factor and its applied lateral distance are determined using the equation. 2.43.

$$f_R = 2.25 \quad [-] \quad (5.2)$$

$$\Delta l = \frac{D_k}{3} = 0.5 \quad [\text{m}] \quad (5.3)$$

From McClung's models, dimensionless creep parameters,  $\frac{L}{H}$ , and the geometrical component,  $D^*$ , have to be assessed.  $D^*$  is set to zero because the glide is null (boundary condition). Using the assignment of the Poisson coefficient made earlier, it is possible to calculate  $\frac{L}{H}$ , from the equation. 2.31. It is equal to 0.3.

Thus, in table 2.2, the parameters relevant to the model's calculation are re-stated:

Parameter	Symbol	Unit	Value
<b>Slope angle</b>	$\psi$	°	30
<b>Creep factor</b> [Swiss Guidelines (2007)]	K	-	0.80
<b>Glide factor</b> [Swiss Guidelines (2007)]	N	-	1
<b>End-effect factor</b> [Swiss Guidelines (2007)]	$f_R$	-	2.25
<b>L/H factor</b> [McClung and Larsen (1989)]	L/H	-	0.3
<b>D* factor</b> [McClung (1982)]	$D^*$	m	0
<b>Height structure perpendicular to slope</b>	$H_{structure}$	m	1.5
<b>Angle between structure and slope</b>	$\alpha_{slope/structure}$	°	90

**Table 5.3:** Snow load device site characteristics

### 5.2.3 Site: Snow supporting structures

In the same way, the second site is considered. It is located on the 35° west-facing slope of Sukkertoppen, directly above the city. The row of avalanche barriers, investigated in this paper, is located in the upper part of Sukkertoppen. These three rows of snow-supporting structures have been implemented in the fall of 2021. Several new rows of barriers are planned to be installed this season. Project implementation is shown on 5.3:



**Figure 5.3:** Sukkertoppen snow support structures

Dimensions of the structures and site parameters have been measured in-situ, see figure 5.3. The ground is considered similar to the shooting range site, with coarse scree. Hence, the glide factor is defined as 1, according to Swiss guidelines, section 2.8. Based on table 2.2, the creep factor is equal to 0.86, because density is set to  $500 \frac{kg}{m^3}$  due to the presence of  $\approx 3m$  snow cover and high wind packing. End-effects are accounted for as follows:

$$f_R = 2.25 \quad [-] \quad (5.4)$$

$$D_K = H_K \cdot \cos(\psi) = 5m \rightarrow \Delta l = \frac{D_k}{3} = 1.67 \quad [m] \quad (5.5)$$

During the design process, the height of the structure is counted as a vertical height between the top of the fences and the ground. Geometrically calculated, the 5m long structure in Sukkertoppen is equal to  $H_K = 6.12m$ .

The characteristics are listed in the table 5.4 below:

Parameter	Symbol	Unit	Value
<b>Slope angle</b>	$\psi$	°	30
<b>Creep factor</b> [Swiss Guidelines (2007)]	K	-	0.86
<b>Glide factor</b> [Swiss Guidelines (2007)]	N	-	1
<b>End-effect factor</b> [Swiss Guidelines (2007)]	$f_R$	-	2.25
<b>Design height structure</b>	$H_K$	m	6.12
<b>Angle between structure and slope</b>	$\alpha_{slope/structure}$	°	50

**Table 5.4:** Sukkertoppen site characteristics

Snow height could not be monitored continuously during the season for this site. Thus, only a maximum height is considered in the calculation, which is  $H_{structure}$ . The objective of this site analysis is to define a maximum snow load, comparing the two guideline models (Swiss and Norwegian) and the snow load estimate based on the snow load device data.

## 5.3 Models evaluation

To finalize the study, it is necessary to analyze and deepen the investigation of the load data. The interpretation of such data is based on the comparison with the models established in the theoretical framework, section 2 and summarized in the table. 2.3.

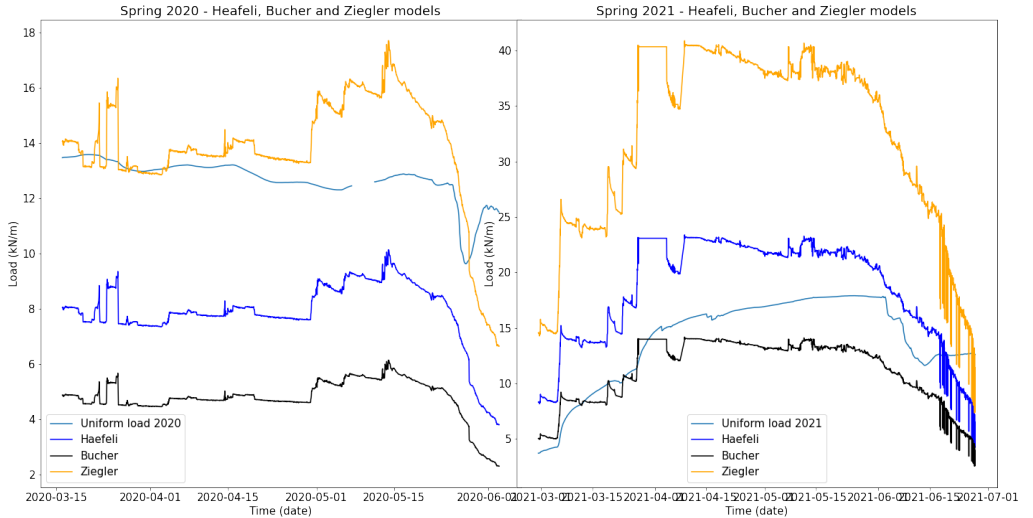
The models are separated into two categories, those created for engineering purposes, Swiss/Norwegian guidelines and McClung/Larsen, and those made for research purposes, Haefeli, Bucher, and Ziegler. The models are compared with load data for the range site, while one design load is compared for the Sukkertoppen snow barriers. The variations in the models are mainly based on the site characteristics and snow depth. Since these are equal for each model, the shape of the plotted models is similar but varies in magnitude. The load data provided by the snow loader for both spring 2020/21 were plotted in four separate graphs, separating the seasons and modeling objectives. The graphs start in March and end in June for spring 2020 and July for spring 2021. Data before March are not considered because well-established pressures in the snowpack are preferred for analysis. There are also gaps in the data set at the beginning of the season.

### 5.3.1 Shooting range

To begin with, research-based models will be examined. These models do not take into account the end-effect pressures. The three models examined have been plotted next to the



uniform load retrieved from apparatus in 4.5.



(a) Research-oriented models - Spring 20

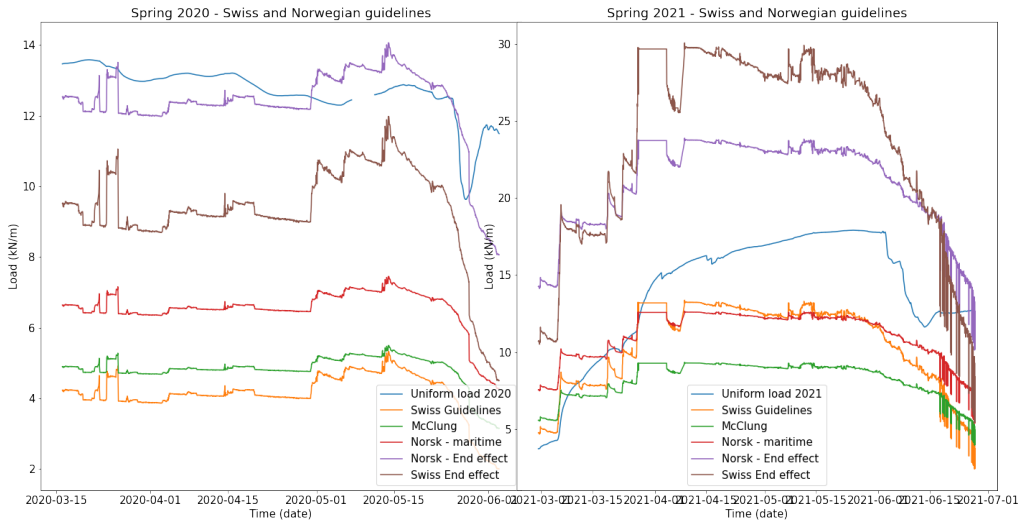
(b) Research-oriented models - Spring 21

**Figure 5.4:** Research-oriented models compared to both springs data

The objective of the representation of these models is to observe their ability to represent the reality of the Svalbardian snowpack pressures. Indeed, these models do not really have a design sizing objective and the representation of reality is sought. However, the age of their formulation also plays a role in their effectiveness in representing reality. As can be seen, the Ziegler model predicts a much higher load than the data collected, see Figure 5.4b, for 2021 spring. This is due to the very simplifying assumptions made in the development of the model, the incompressibility and homogeneity of the snowpack, as well as the squared rise in snow height. Yet, in 2020, it represents the data set quite well, which could suggest a less compressible and more homogeneous snowpack in Svalbard. However, it is impossible to express more than a thought at this stage. As for the model, Bucher (1948), it underestimates the loads in the spring of 2020 by a large margin and barely matches the data for 2021. The main reason for this difference is the fact that the model is working better for low densities. Finally, the plot for the year 2020 is also quite far from the reality of the data. It is interesting to know how it behaves, as it is the basis of many research (mainly Swiss standards). The reason behind the difference in the magnitude of the model results between the two springs is exposed in the following

paragraph.

In the design-oriented graphs, figure. 5.5, the three models have been plotted, with the addition of the end effect accounting for Swiss and Norwegian standards. As a reminder, the placement of the load cells on the snow wall leads to the measurement of these end effects.



(a) Guidelines models - Spring 20

(b) Guidelines models - Spring 21

**Figure 5.5:** Guidelines models compared to both springs data

To begin with, it is easy to see the impact of the end-effect factor on the loads. In the case of spring 2020, the simple models largely underestimate the linear forces developed by the snowpack. Swiss Guidelines (2007) and McClung and Larsen (1989) evaluate a load of more than half of the reality and Larsen (2000), taking into account the maritime environment, does a little better but remains too low.

It should be noted that despite the different approaches taken by McClung and the Swiss researchers, their estimates are very close, figure. 5.5a. The two models show load curves further apart in 2021 in the 5.5b model, but this is due to the snow cover being much deeper in 2021 than the monitored plate height. All the models' pressures for this 2021 season are overestimated for this reason. Since the Swiss guidelines take into account the square of the snow depth, this has a considerable influence on the model results. As can be seen at the end of the season, for both years the Swiss models decrease much faster than the other

models and the data. This is due to a rapid loss of snow height at this period, but which does not necessarily mean a rapid loss of pressure, as the data show. Thus, the 2020 data are more interesting to compare because the maximum height of the snow cover is closer to that of the wall.

Now, focusing on the end effects on structures, the Swiss guidelines are much lower than what is measured by the load device. For the design, this would not be acceptable. There is an additional factorisation by safety factors, as we will see in the next section, but this is not enough to mark up data correctly. On the other hand, the end effects associated with a definition of the marine environment, by Larsen (2000), are close to the data curve and, with the safety factors, could be adequate to define a design load for this case.

### 5.3.2 Sukkertoppen

The purpose of this section is to compare the dimensional load difference on the new structures implemented on Sukkertoppen. As mentioned in the introduction, the study of the Sukkertoppen structures was scaled down due to complications with the permit approvals and manufacturing of the pressure plate. Therefore, this section will only present the results of the models applied to the site, including the design factors. The characteristics of the site and the structures have been described in the previous chapter. The models chosen for the comparison are the engineering ones, i.e. the Swiss and Norwegian standards. The rows of fences are continuous, that is to say, the end-effects are present only on two sides for each row and are of the maximal value, only depending on the glide factor, as defined in equation 2.43. A study of the implications of the design requirement will be made. The design criteria, used by the Swiss guidelines and presented in the section 2.5 and in equation 2.42, will be followed in this subchapter.

Model	Unit	Value
Swiss	kN/m	80.9
Swiss - End effect	kN/m	182.1
Norwegian - Maritime	kN/m	51.3
Norwegian - End effect	kN/m	95.7
McClung	kN/m	20.2
Design: $E_d$ [Swiss]	kN/m	121.2
$\Delta l$	m	2.04

**Table 5.5:** Load calculation Sukkertoppen snow support structures

The height of the structure is much higher than one of the plates, which leads to bigger

differences between the Swiss and the other guidelines in this analysis. The end effect is roughly 90% higher for the Swiss compared to the Norwegians. When designing for variable actions, the factor established by the Eurocode, the Swiss end effect of the actions,  $E_d$ , becomes much more dimensional. Unfortunately, the lack of in situ monitoring of snow pressures/loads prevents the verification of model results. It would have been interesting to know loads of an accumulated snow cover on the structures. The location is also more exposed to wind action than the snow load device studied.

## Conclusions & Further work

The pressures within the snowpack and subsequently the linear loads on a structure in sloping terrain are influenced by many parameters, those specific to the site, and those that change over the season and position in the world. In Svalbard, it has been shown that load variations are most sensitive to the temperature gradient and cumulative creep. The direct influence of external temperature on creep has been touched upon but the lack of consistent snow temperature data, in 2022, prevents more reliable conclusions.

The maximum load amplitude is mainly controlled by the snow depth and snow-pack density. Thus, from a design point of view, priority is often given to the evaluation of these parameters, with the characteristic snow depth defining the height of the structure and the other parameters contributing to the definition of the required strength of the structure.

To this end, the models presented and used in this work have allowed us to question their representative value for a Svalbardian pack. The end-effect has a very sizing effect for these calculations but is necessary because it is the only way to obtain a mark-up of the loads measured in-situ. Glide also has a strong contribution to the final load results and not taking it into account reduces them considerably. The Norwegian and the Swiss guidelines have provided conclusive results based on the data collected. However, there are some differences in their approach. The Swiss standards are mainly relying on the snow height considered, which increases the loads considerably for high snow heights, but for low snow heights, it tends to underestimate a lot the pressures. In this respect, the Norwegian standards seem to be more consistent with the data. The low precipitation and snowfall in Svalbard, compared to the Swiss Alps, puts the importance of the snow height parameter into perspective, which would lead to the possibility of over or under-sizing the

---

structures. The choice is often also dictated by economic and structural/foundation optimization considerations. On this matter, the wishes of the client and the constraints of the design offices come into a discussion.

The extremely changeable weather conditions in recent years in Svalbard make it necessary to consider a probable increase in the temperature gradient and creep, which so far have remained low in the measured data. In addition, the spring of 2022 has shown that strong warming periods, mid-winter, are not exempt anymore in the High Arctic and that their impacts need to be taken into account.

Further analysis of meteorological data alongside creep and temperature gradient measurements would be an interesting avenue for further work. In situ data on snow creep are scarce worldwide, and even more so in the Arctic. Its influence on materials as porous as snow is considerable. As mentioned earlier, Svalbard is experiencing a warming climate like nowhere else on the planet, and studying the impact of this evolution on the snowpack pressure development would provide valuable information for other alpine regions.

Moreover, the temperature gradient in the snowpack showed a significant impact on the load. Its introduction into the linear force model, alongside the creep factor, would be beneficial for the representation of the snowpack behavior. Finally, in continuation of the data collection campaign in Norway and the USA, the implementation of monitored avalanche structures on Sukkertoppen would provide valuable data for the development of new models or verification of existing models, and for comparison with creep and density data at the same location.

# Bibliography

- Abe, O., 2001. Creep experiments and numerical simulations of very light artificial snow-packs. *Annals of Glaciology* 32, 39–43. doi:10.3189/172756401781819201.
- Alberg, A., 2019. Snow load device system.
- B, A., Haider, S., 2016. Parameterization experiment on the effect of temperature on snow albedo and snow .
- Bader, H., Salm, B., 1990. On the mechanics of snow slab release. *Cold Regions Science and Technology* 17, 287–300. URL: <https://www.sciencedirect.com/science/article/pii/S0165232X05800072>, doi:[https://doi.org/10.1016/S0165-232X\(05\)80007-2](https://doi.org/10.1016/S0165-232X(05)80007-2).
- Bader H, Hansen BL, J.J.S.M., 1951. Preliminary investigations of some physical properties of snow.
- Bartelt, P., Christen, M., Wittwer, S., 2000. Program haefeli - two-dimensional numerical simulation of the creeping deformation and temperature distribution in a phase changing snowpack. *Snow Engineering: Recent Advances and Developments* , 13–22.
- Bucher, E., 1948. Beitrag zu den theoretischen Grundlagen des Lawinenverbaus.
- Caselli, N., 2004. Field measurement of snow creep in a radiation snow climate, san juan mountains, colorado .
- Christiansen, H., Humlum, O., Eckerstorfer, M., 2013. Central svalbard 2000-2011 meteorological dynamics and periglacial landscape response. *Arctic, Antarctic, and Alpine Research* 45, 6–18. doi:10.1657/1938-4246-45.16.

- 
- Colbeck, S.C., 1987. Snow metamorphism and classification. *Seasonal Snowcovers: Physics, Chemistry, Hydrology*, 1–35doi:10.1007/978-94-009-3947-9\_1.
- De Quervain, M., 1945. Die setzung der schneedecke, in: *Interner Bericht Nr. 11, Eidgenössisches Institut für Schnee- und Lawinenforschung*,.
- Eckerstorfer, M., 2013. Snow avalanches in central Svalbard: A field study of meteorological and topographical triggering factors and geomorphological significance. Ph.D. thesis.
- Gubler, H., 1994. Physik von schnee, in: *Skriptum. Eidgenössisches Institut für Schnee- und Lawinenforschung*.
- Haefeli, R., 1948. *Schnee, Lawinen, Firn und Gletscher*. Springer Vienna, Vienna. pp. 663–735. URL: [https://doi.org/10.1007/978-3-7091-5845-6\\_13](https://doi.org/10.1007/978-3-7091-5845-6_13), doi:10.1007/978-3-7091-5845-6\_13.
- Haefeli, R., Bader, H., Neher, J., Eckel, O., Thams, C., Bucher, E., 1939. *Der Schnee und seine Metamorphose*. Beitr. Geol. Schweiz. Geotek. Hydrologie, Kommissionsverlag Kümmerly & Frey, Druck von Aschmann & Scheller a.-g., Zürich. URL: <https://books.google.com/books?id=yHEetAEACAAJ>.
- Harada, Y., 2014. Changes in design standards and regional characteristics of avalanche supporting structures in japan.
- Hestnes, E., 2018. Longyearbyen, svalbard - vulnerability and risk management of an arctic settlement under changing climate - a challenge to authorities and experts.
- Hewes, J.T., Decker, R., Merry, S., Strain, S., 2016. Design and performance monitoring of snow-supporting structures for the milepost 151 avalanche near jackson, wyoming. *Transportation Research Record* 2551, 118–125. doi:10.3141/2551-14.
- Indreiten, M., 2018. The longyearbyen fatal avalanche accident 19th december 2015, svalbard - lessons learned from avalanche rescue inside a settlement.
- Kuhn, W., 1939. Beziehungen zwischen viscosität und elastischen eigenschaften amorpher stoffe. *Zeitschrift für Physikalische Chemie* 42B, 1–38. URL: <https://doi.org/10.1515/zpch-1939-4202>, doi:doi:10.1515/zpch-1939-4202.
- Larsen, J., 2000. Design criteria for avalanche supporting structures exposed to snow creep forces in maritime climate. *Snow Engineering: Recent Advances and Developments*, 109–112.



- 
- Larsen, J.O., McClung, D.M., Hansen, S.B., 1985. The temporal and spatial variation of snow pressure on structures. *Canadian Geotechnical Journal* 22, 166–171. doi:10.1139/t85-023.
- Lonardi, 2018. Characterization of wind channeling around longyearbyen, svalbard.
- M, D.Q., 1966. Measurements on the pressure at rest in a horizontal snow cover.
- Margreth, S., 2016. New technical guideline on snow supporting structures in avalanche starting zones .
- McClung, 1975. Creep and the snow—earth interface conditions in the seasonal snowpack.
- McClung, Schaerer, 2006. Avalanche handbook .
- McClung, D., Larsen, J., 1989. Snow creep pressures: Effects of structure boundary conditions and snowpack properties compared with field data. *Cold Regions Science and Technology* 17, 33–47. URL: <https://www.sciencedirect.com/science/article/pii/S0165232X8980014X>, doi:[https://doi.org/10.1016/S0165-232X\(89\)80014-X](https://doi.org/10.1016/S0165-232X(89)80014-X).
- McClung, D.M., 1982. One-dimensional analytical model for snow creep pressures on rigid structures. *Canadian Geotechnical Journal* 19, 401–412.
- Mellor, M., 1975. A review of basic snow mechanics.
- Navarre, J.P., Meyssonier, J., Vagnon, A., 2007. 3d numerical model of snow deformation without failure and its application to cold room mechanical tests. *Cold Regions Science and Technology* 50, 3–12. URL: <https://www.sciencedirect.com/science/article/pii/S0165232X07000766>, doi:<https://doi.org/10.1016/j.coldregions.2007.04.002>. snow and Avalanches EGU 2006.
- Norem, H., 2014. Veger og snøskred.
- Overland, J., Dunlea, E., Box, J.E., Corell, R., Forsius, M., Kattsov, V., Olsen, M.S., Pawlak, J., Reiersen, L.O., Wang, M., 2019. The urgency of arctic change. *Polar Science* 21, 6–13. URL: <https://www.sciencedirect.com/science/article/pii/S1873965218301543>, doi:<https://doi.org/10.1016/j.polar.2018.11.008>. iSAR-5/ Fifth International Symposium on Arctic Research.

- 
- Perla, R., 1977. Slab avalanche measurements. *Canadian Geotechnical Journal* 14, 206–213. doi:10.1139/t77-021.
- Perla, R.I., 1972. Generalization of haefeli's creep-angle analysis. *Journal of Glaciology* 11, 447–450. doi:10.3189/S0022143000022395.
- R, H., 1966. Considerations sur la pente critique et le coefficient de pression au repos de la couverture de neige.
- Salm, B., 1977. Snow forces. *Journal of Glaciology* 19, 67–100. doi:10.3189/S0022143000029221.
- Schweizer, J., 1999. Review of dry snow slab avalanche release. *Cold Regions Science and Technology* 30, 43–57. URL: <https://www.sciencedirect.com/science/article/pii/S0165232X99000257>, doi:[https://doi.org/10.1016/S0165-232X\(99\)00025-7](https://doi.org/10.1016/S0165-232X(99)00025-7).
- Shapiro, e.a., 1997. Snow mechanics: Review of the state of knowledge and applications , 40.
- Singh, A.K., 2011. *Snow Metamorphism*. Springer Netherlands, Dordrecht. pp. 1060–1061. URL: [https://doi.org/10.1007/978-90-481-2642-2\\_675](https://doi.org/10.1007/978-90-481-2642-2_675), doi:10.1007/978-90-481-2642-2\_675.
- Sommerfeld, R.A., LaChapelle, E., 1970. The classification of snow metamorphism. *Journal of Glaciology* 9, 3–18. doi:10.3189/S0022143000026757.
- Swiss Guidelines, S., 2007. Defense structures in avalanche starting zones: Technical guideline as an aid to enforcement.
- Teufelsbauer, H., 2011. A two-dimensional snow creep model for alpine terrain. *Natural Hazards* 56, 481–497. doi:10.1007/s11069-010-9515-8.
- Walker, W., 1994. Snow creep movement in the san juan mountain snowpack .
- Yoshida, 1963. Physical properties of snow. ice and snow: processes, properties and applications.
- Ziegler, H., 1963. Methoden der plastizitätstheorie in der schneemechanik. *Zeitschrift Für Angewandte Mathematik Und Physik Zamp* 14, 713–737. doi:10.1007/BF01601164.
- Ziegler, H., 1975. Continuum mechanics: a powerful tool in solving ice and snow problems, in: *Snow Mechanics Symposium*.
-

---

# Appendix

## 6.1 Appendix A

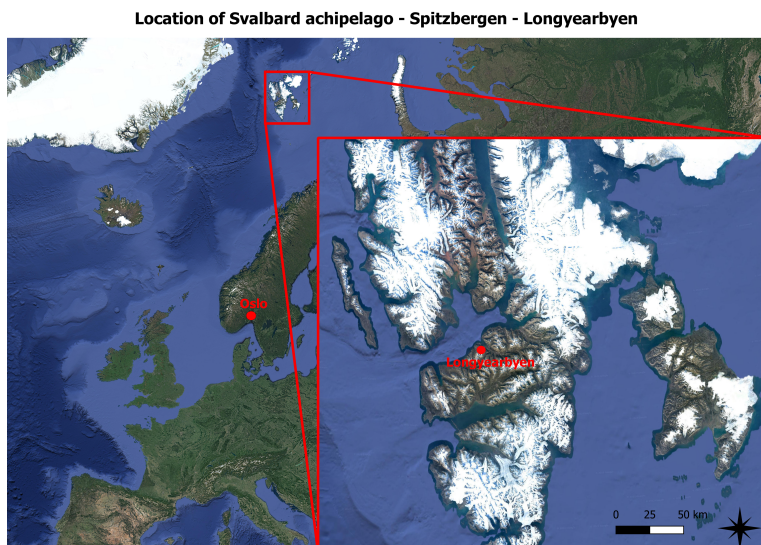


**Figure 6.1:** Location of Svalbard archipelago

---

## 6.2 Appendix B

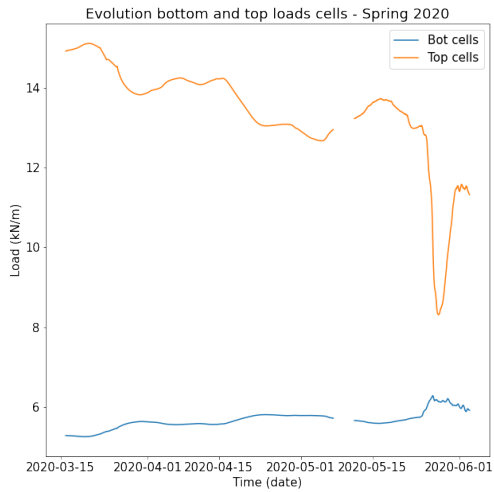


**Figure 6.2:** Load cells - Spring 2020

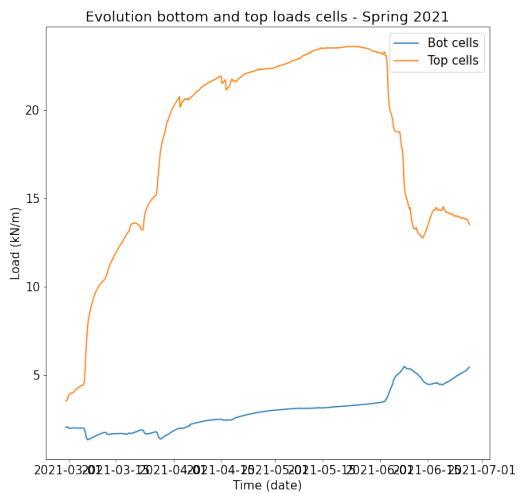


**Figure 6.3:** Load cells - Spring 2021

## 6.3 Appendix C

A more realistic definition of the distributed load would be to assume a progressively higher load towards the surface, as recorded by the snow loading device. The literature suggests a parabolic load distribution, but this is not controllable by the snow load device, i.e. there are no cells in the middle of the plate.

Assume a load distributed as shown in the figure 6.4,

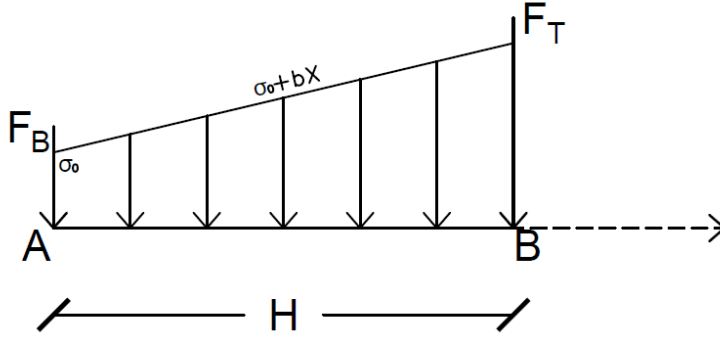


Figure 6.4: More realistic load distribution over the studied plate

The distributed load,  $\sigma$ , over the depth,  $x$ , is defined as follows.  $b$  being a constant to determine.

$$\sigma(x) = \sigma_0 + b \cdot x \quad (6.1)$$

If the sum of the bending moments at point A (bottom of the plate) is calculated. The force measured at the top of the plate times the lever arm must be equal to the resultant of the distributed load times its lever arm.

$$\sum M_A = 0 \rightarrow \int_0^H \sigma(x) \cdot x \cdot dx = F_T \cdot H \quad (6.2)$$

$$\Rightarrow \int_0^H (\sigma_0 + b \cdot x) \cdot x \cdot dx = F_T \cdot H \quad (6.3)$$

$$\Rightarrow \int_0^H \sigma_0 \cdot x \cdot dx + \int_0^H b \cdot x^2 \cdot dx = F_T \cdot H \quad (6.4)$$

$$\Rightarrow \sigma_0 \cdot \frac{x^2}{2} \Big|_0^H + b \cdot \frac{x^3}{3} \Big|_0^H = F_T \cdot H \quad (6.5)$$

$$\Rightarrow \sigma_0 \cdot \frac{H^2}{2} + b \cdot \frac{H^3}{3} = F_T \cdot H \quad (6.6)$$

---

And the sum of the shear forces is also zero, so:

$$\sigma_0 \cdot H + b \cdot \frac{H}{2} - F_T - F_B = 0 \quad (6.7)$$

Knowing the values of  $H$ ,  $F_B$  and  $F_T$ , we end up with two equations containing two unknowns, easily solvable.

---

## 6.4 Appendix D

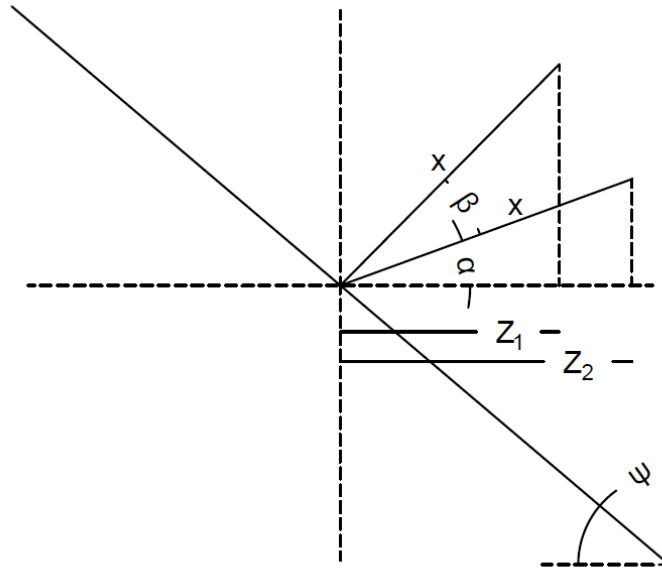


**Figure 6.5:** Creep calculation

Creep calculation using the geometry of the experiment:

$$\cos(\beta) = \frac{z1}{x} \quad (6.8)$$

$$\cos(\alpha) = \frac{z2}{x} \quad (6.9)$$

$$\Rightarrow z2 - z1 = x \cdot (\cos(\alpha) - \cos(\beta)) \quad (6.10)$$



**Figure 6.6:** Poles broken - North side



**Figure 6.7:** Stake n°1 breakage - June 2022



---

## 6.5 Appendix E

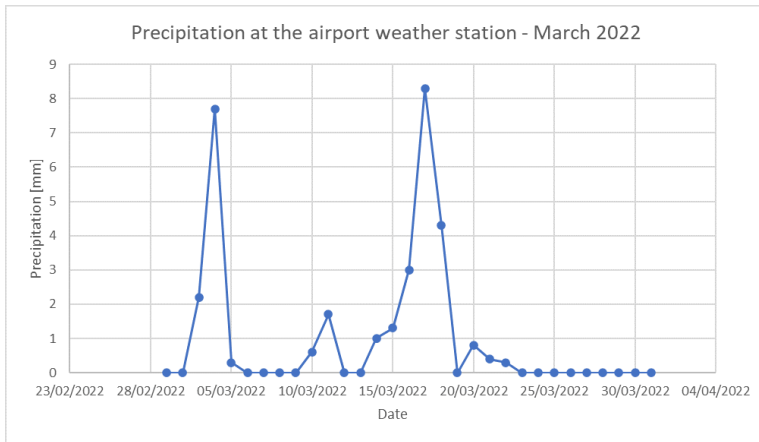


**Figure 6.8:** Rain event - Airport Weather Station - March 2022

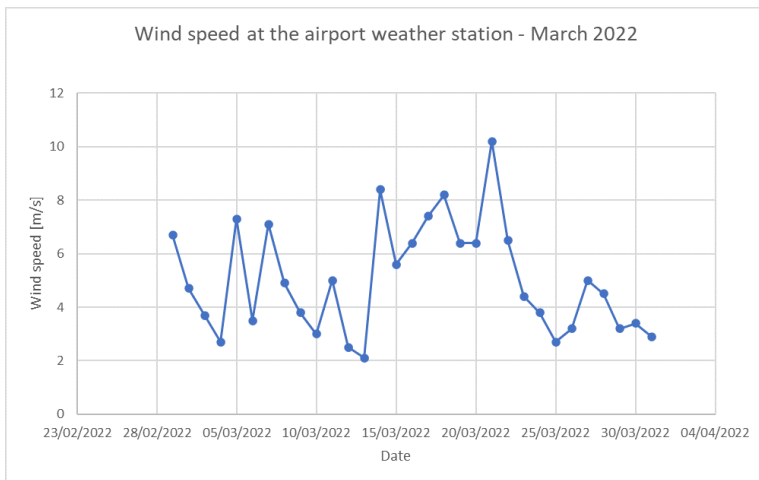


**Figure 6.9:** Wind speed - Airport Weather Station - March 2022

